Physics – Uspekhi **41** (9) 843 – 863 (1998)

REVIEWS OF TOPICAL PROBLEMS PACS numbers: **74.20.–z**, **74.72.–h**, **74.90.+n**

Surface impedance of HTSC single crystals in the microwave band

M R Trunin

Contents

Abstract. Currently available data on the real, R_s, and imaginary, X_s, parts of the microwave frequency surface impedance $Z_s = R_s + iX_s$ are presented for the high-quality single-crystal high-temperature superconductors $YBa_2Cu_3O_{6.95}$, $Ba_{0.6}K_{0.4}BiO_3$, $Tl_2Ba_2CaCu_2O_{8-\delta}$, $Tl_2Ba_2CuO_{6+\delta}$, and $Bi_2Sr_2CaCu_2O_8$. A high-precision technique for measuring the temperature dependences $R_s(T)$ and $X_s(T)$ in the range $4.2 \leqslant T \leqslant 150$ K is described. Surface impedance and complex conductivity features common to single-crystal high-temperature superconductors are formulated and the temperature variation of these properties is analyzed. To explain the experimental data, a modified two-fluid model is used, which includes quasi-particle scattering and accounts for the characteristic change in the density of superconducting carriers at low and near-critical temperatures. Prospects for the microscopic theory of the high-frequency response of high-temperature superconductors are discussed.

1. Introduction

The superconducting interaction and symmetry of the order parameter in high-temperature superconductors (HTSC) are the subjects of wide speculation and much controversy. Among the experimental methods of studying these problems is the microwave measurement of the surface impedance $Z_s(T) = R_s(T) + iX_s(T)$ of HTSC single crystals at various temperatures T. The results yield information about the scattering mechanism, the density of states, and the nature of superconducting pairing in the compounds.

The real part of the impedance, the surface resistance R_s, determines the energy losses of an electromagnetic wave reflected from the superconductor. Typical values of the surface resistance fall in the range $0.1 < R_s < 0.4\ \Omega$ for the centimeter wave band and the normal state of HTSC single crystals near the transition temperature T_c. When the sample becomes superconducting, the surface resistance sharply decreases, but does not vanish in experiments even as $T \to 0$. The residual surface resistance $R_{res} \equiv R_s(T \to 0)$ depends on various surface defects. This fact, which was revealed as early as in experiments with conventional superconductors, suggests that the lower R_{res}, the higher the quality of samples. Below we will consider single-crystal $YBa_2Cu_3O_{6.95}$ (YBCO), $Ba_{0.6}K_{0.4}BiO_3$ (BKBO), $Tl_2Ba_2CaCu_2O_{8-\delta}$ (TBCCO), $Tl_2Ba_2CuO_{6+\delta}$ (TBCO) and $Bi_2Sr_2CaCu_2O_8$ (BSCCO) samples, which are stoichiometrically perfect and have a transition temperature corresponding to optimal doping; the transition width ΔT_c, determined by surface resistance measurements, is small, $\Delta T_c \lesssim 1$ K, and the residual surface resistance R_{res} does not exceed several mΩ at microwave frequencies $f \sim 10$ GHz†. There is good reason to believe that the electrodynamic quantities measured in these samples correspond to intrinsic microscopic properties of the superconductor.

The imaginary part of the surface impedance, the reactance X_s, determines the nondissipative energy stored in

M R Trunin Institute of Solid-State Physics, Russian Academy of Sciences, 142432 Chernogolovka, Moscow Region, Russia
Tel. (7-095) 742 01 42 (ext. 29-42)
Fax (7-095) 576 41 11
E-mail: trunin@issp.ac.ru

Received 16 February 1998
Uspekhi Fizicheskikh Nauk **168** (9) 931 – 952 (1998)
Translated by G N Chuev; edited by A Radzig

† At present, extremely low values of $R_{res} \simeq 10\ \mu\Omega$ have been observed in YBCO single crystals at frequencies ~ 10 GHz.

the surface layer of the superconductor. Using the International System of Units, we have $X_s(T) = \omega\mu_0\lambda(T)$ at $T < T_c$, where $\omega = 2\pi f$, $\mu_0 = 4\pi \times 10^{-7}$ H/m, and $\lambda(T)$ is the depth of magnetic field penetration into the superconductor.

It is well known that the superconducting state of an HTSC is characterized by an extremely short coherence length ξ_0 dictating the scale of electron pair correlation. The inequality $\xi_0 \ll \lambda$, which is valid at $T < T_c$ in an HTSC, means that the field is constant over a length of ξ_0, hence we can use a simple local equation

$$Z_s = R_s + iX_s = \left(\frac{i\omega\mu_0}{\sigma_1 - i\sigma_2}\right)^{1/2} \tag{1}$$

to relate the impedance and complex conductivity $\sigma_s = \sigma_1 - i\sigma_2$ of the superconductor. From Eqn (1) we find the expressions for the real σ_1 and imaginary σ_2 parts of the conductivity

$$\sigma_1 = \frac{2\omega\mu_0 R_s X_s}{(R_s^2 + X_s^2)^2}\,, \qquad \sigma_2 = \frac{\omega\mu_0(X_s^2 - R_s^2)}{(R_s^2 + X_s^2)^2}\,. \tag{2}$$

Above the transition temperature, the mean free path l of carriers is small with respect to the skin depth δ, i.e. $l \ll \delta$, meaning the condition of the normal skin effect. Equations (1) and (2) also describe the normal state of an HTSC at $T \geqslant T_c$, where $R_s(T) = X_s(T) = \sqrt{\omega\mu_0/2\sigma_n(T)}$, $\sigma_n \equiv \sigma_1(T \geqslant T_c)$, and $\sigma_2 = 0$.

Measurements of the temperature dependences $Z_s(T)$ in absolute units allow one to calculate $\sigma_s(T)$ and provide an experimental test for any phenomenological and microscopic models describing electromagnetic properties of superconductors. The dependences obtained in the study of the early high-quality YBCO single crystals did not agree with the Bardeen – Cooper – Schrieffer (BCS) theory [1].

At frequencies much less than the energy gap Δ, i.e. $\hbar\omega \ll \Delta$, the BCS model predicts two peculiarities of the microwave response in superconductors [1 – 3]: at $T < 0.5T_c$, the real part of conductivity $\sigma_1(T)$ decreases exponentially and the surface resistance $R_s(T) \propto \exp[-\Delta(0)/kT]$, while at temperatures in the interval $0.8 < T/T_c \leqslant 1$ the conductivity $\sigma_1(T)$ increases with respect to its value σ_n in the normal state. The first peculiarity results from the activation dependence of the derivative $d\Delta(T)/dT$ for $T \ll T_c$, while the second feature is due to the singularity in the density of states when the elementary excitation energy is comparable with the gap $\Delta(T)$. The exponential dependence $R_s(T)$ has been detailed for conventional superconductors (see, for example, Ref. [4] and references therein). The peak of $\sigma_1(T)$ around $T \sim 0.85T_c$ (referred to as the coherent peak) was detected only recently in Nb and Pb samples on a frequency of 60 GHz [5], and in Nb on a frequency of 10 GHz [6], realized for simultaneous measurements of temperature dependences $R_s(T)$ and $X_s(T)$ with a high precision.

Increasing the electron-phonon coupling constant leads to suppression of the singularity in the density of states of a superconductor at $\hbar\omega = \Delta$, as follows from the generalized BCS theory developed by Eliashberg [7]. As a result, the amplitude of the coherent peak decreases and, according to Ref. [8], virtually disappears at frequencies ~ 10 GHz when the electron-phonon coupling constant exceeds unity. The inset to Fig. 1 shows the dependences $\sigma_1(T)/\sigma_1(T_c)$ calculated using the isotropic BCS and strong coupling (SC) models. The narrow peak in Fig. 1 detected by microwave measurements

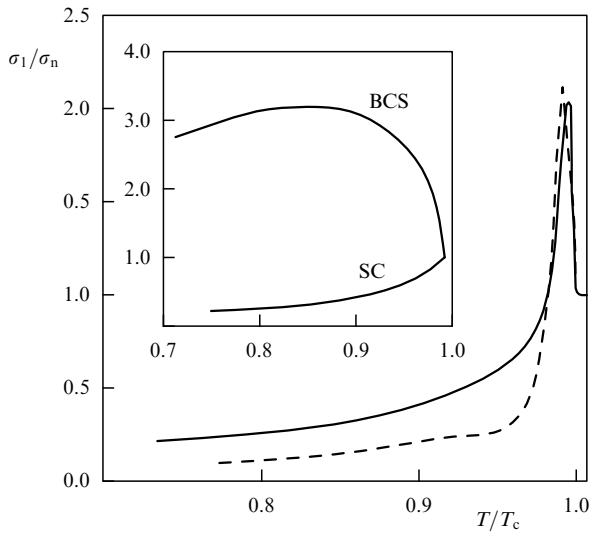

Figure 1. Comparison of the experimental dependence σ_1/σ_n (dashed line, YBCO crystal) and that calculated with the SC model (solid line) taking into account the inhomogeneous broadening of the superconducting transition. The inset shows the temperature dependences σ_1/σ_n calculated with the BCS and SC models [10].

of $\sigma_1(T)$ in HTSC single crystals around T_c can be caused by inhomogeneous broadening of the superconducting transition [9, 10] or can result from fluctuation effects [11, 12]. Another consequence of the SC model is that the temperature dependences $R_s(T)$ [13] and $\lambda(T)$ [14] are not exponential. Power temperature dependences are also obtained in the framework of the well-known two-fluid Gorter – Casimir (GC) model [15]. Near the transition temperature they look like the dependences calculated from the SC model [16]. However, especially in the low-temperature range the quantitative difference between these dependences and those experimentally established in HTSC single crystals was found to be huge. For example, it is seen from Fig. 2 where the temperature dependence $\Delta\lambda_{ab}(T)$ measured in the *ab*-plane of YBCO [17] is compared with that found from isotropic BCS and SC models [18]. In the scale of the figure the curve

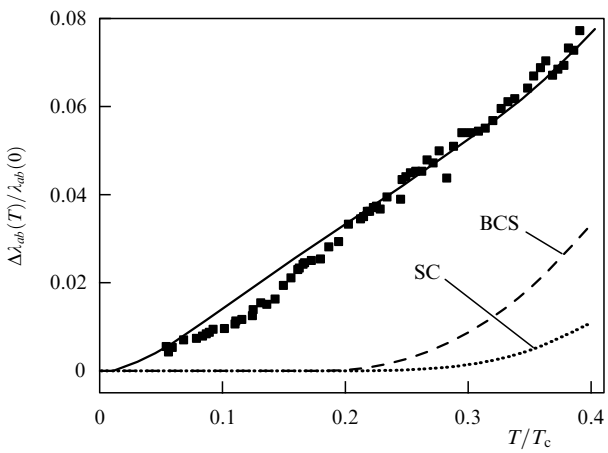

Figure 2. Low-temperature dependence $\Delta\lambda_{ab}(T)$: the squares correspond to the experimental data taken from Ref. [17]; the solid line plots the data calculated using the two-band model [18] (see Section 5); the dashed line presents the results obtained with the isotropic BCS model, and the dotted line corresponds to the data calculated using the isotropic SC model.

corresponding to the phenomenological GC model would appear as a horizontal line.

The first high-quality YBCO single crystals were produced by a research group from The University of British Columbia (UBC, Vancouver) [19], which detected two special features of the temperature dependence $Z_s(T)$ for these crystals:

(a) the linear temperature dependence of the penetration depth over the interval $0 < T < T_c/3$ [20];

(b) the surface resistance linearly depends on the temperature over the range $T < T_c/3$ and has a wide peak centred near $T_c/2$ [21].

Both these experimental features appeared surprising from the point of view of conventional models for the high-frequency response of superconductors. They provoked a lengthy discussion about the symmetry of the order parameter, the relaxation of quasi-particles, interband and intraband effects, and, as a result, enabled most of the probable mechanisms of superconducting pairing in HTSC crystals to be revealed. By now the results (a) and (b) have been confirmed in experiments on YBCO crystals by researchers from other laboratories. The data obtained recently from high-quality BSCCO, BKBO, TBCCO and TBCO single crystals allow us to determine the peculiar and common features of the temperature dependences of the impedance and conductivity of various HTSC single crystals.

We begin our review with the description of the experimental technique used for precise measurements of the temperature dependences of the surface impedance of HTSC single crystals in the microwave range (Section 2). The corresponding measurement results are listed and systematized in Section 3. Section 4 is devoted to a comparison of the experimental dependences $Z_s(T)$ and $\sigma_s(T)$ with the data calculated in the framework of the modified two-fluid model. Finally, in Section 5 we shall discuss microscopic theories, the possible symmetry and multicomponent nature of the order parameter, which are revealed by the above measurements on the microwave response in crystalline HTSCs.

2. Measuring the impedance of small-sized superconductors in the microwave band

The surface impedance of small-sized HTSC samples, whose surface is about 1 mm^2, is most conveniently measured by applying the technique developed in Ref. [22]. According to this approach, a sample is held by a sapphire rod at the centre of a cylindrical superconducting cavity resonating in the H_{011} mode, i.e. at the maximum of a homogeneous microwave magnetic field. By varying the temperature of the sapphire rod and measuring first the Q-factor and the frequency shift Δf of the cavity with the sample inside and then those of the empty cavity (Q_0, Δf_0), one can determine the surface resistance R_s and the reactance X_s of the sample as functions of temperature.

The method requires that the experimental facility should satisfy two basic conditions. Firstly, since HTSC single crystals are small and their losses in the superconducting state are low, the empty cavity should have a high Q-factor so that the temperature dependence of the sample impedance can be detected against the background of the cavity parameters. Secondly, the measurements of Q and Δf by sweeping the frequency require the microwave generator to be highly stable.

2.1 The experimental setup

We employed a cylindrical resonating cavity with a diameter and height of 42 mm fabricated from niobium (Fig. 3). The cavity was immersed in liquid helium, so its material was always in the superconducting state. The H_{011} mode was driven at a frequency of 9.42 GHz. The field configuration for this mode was suitable for measuring the microwave properties in a small sample located in the centre of the cavity, where the microwave magnetic field was homogeneous and parallel to the cylinder axis. Since the H_{011} mode is degenerate (the E_{111} mode has the same frequency), niobium posts with a diameter and a height of 5 mm were made on both the upper and lower lids of the cavity, which resulted in a difference between the E_{111} and H_{011} modes of more than 50 MHz. An important feature of the cavity unit was the possibility of smoothly changing the coupling between the waveguides and the cavity, which allowed us to obtain the required coupling constants over a wide range of Q-factor. The sapphire rod supporting the sample was thermally insulated from the cavity walls owing to the high-vacuum condition inside the cavity, which was sealed by indium rings. The lower end of the sapphire rod was inserted into a stainless-steel tube, which was, in turn, supported by an aligning Teflon mandrel. This thermal insulation allowed the cavity Q-factor to be maintained at a level of about 10^7 when the temperature of the sample and rod was $T \sim 150$ K.

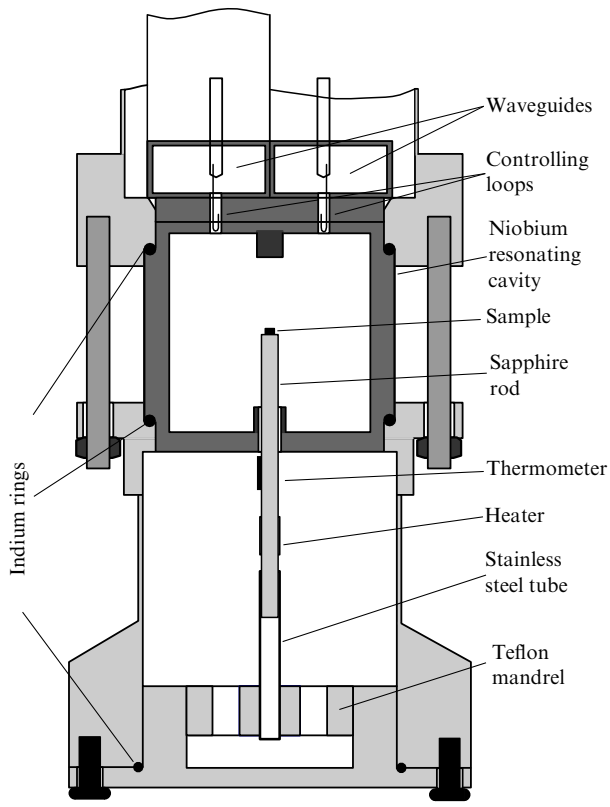

Figure 3. Design of the microwave cavity unit.

2.2 The measuring scheme

The sample temperature was controlled by the circuit shown in Fig. 4. Experimental data from the thermometer T were processed by an analog-digital converter (ADC) and fed to a computer. The latter compared the measured and prescribed temperatures and transmitted the difference signal to a

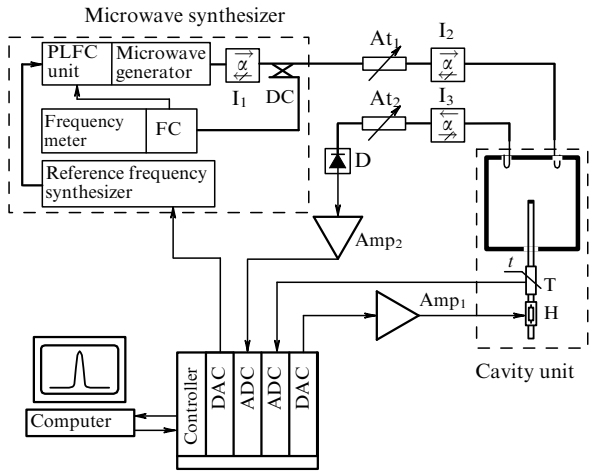

Figure 4. Layout of the facility for measuring the Q-factor and shift of the resonance frequency as functions of temperature.

digital-analog converter (DAC). The resulting driving signal was fed to an amplifier Amp1 and corrected the thermal power generated by a heater (H). The temperature was maintained at the prescribed value to within 0.3% throughout the entire temperature range $4 < T < 150$ K.

The high stability ($\approx 10^9$) of the microwave frequency was ensured by a microwave synthesizer equipped with a phase-locked frequency control (PLFC) loop. The microwave signal was fed through an isolator I1; then a fraction of the microwave power was diverted out by a directional coupler (DC) and conducted to a frequency converter (FC). There the oscillations with frequency 9.4 GHz were transformed to a lower-frequency band (up to 50 MHz) and fed to a PLFC unit, where the lower frequency was compared with that generated by a reference frequency synthesizer in the megahertz band. Thus a signal proportional to the phase difference was produced to drive the microwave generator, and the feedback loop was closed. The frequency was controlled by sweeping the frequency of the reference synthesizer, which was driven by the output of a 20-bit DAC.

An electromagnetic wave generated by the microwave synthesizer was transmitted over a rectangular waveguide through the attenuator At1 and isolator I2 to the cavity coupled to the waveguides through tunable coupling loops. At the output of the cavity, the wave was conducted through an isolator I3 and attenuator At2 to diode D operating in the quadratic regime, which was carefully controlled. The diode output amplified by an amplifier Amp2 was converted by an ADC and fed to the computer.

In the presence of energy losses, the induced oscillations of the resonating cavity are characterized by the complex frequency [23]

$$\hat{\omega}_{\mathrm{i}} = \omega_{\mathrm{i}} + \frac{\mathrm{i}\omega_{\mathrm{i}}}{2Q_{\mathrm{iL}}}\,, \tag{3}$$

where $\omega_{\mathrm{i}} = 2\pi f_{\mathrm{i}}$ and Q_{iL} are the eigen-frequency and the loaded Q-factor of the cavity, respectively. For the transmission-mode cavity used in our experiments the Q-factor is

$$\frac{1}{Q_{\mathrm{iL}}} = \frac{1}{Q_{\mathrm{i}}} + \frac{1}{Q_1} + \frac{1}{Q_2}\,, \tag{4}$$

where Q_{i} is the unloaded Q-factor, Q_1 and Q_2 are the input and output Q-factors determining the coupling between the cavity and waveguides. In Eqns (3) and (4), $Q_{\mathrm{iL}} = Q_{\mathrm{L}}$, $Q_{\mathrm{i}} = Q$ and $f_{\mathrm{i}} = f$ when the sample is held in the cavity, and $Q_{\mathrm{iL}} = Q_{0\mathrm{L}}$, $Q_{\mathrm{i}} = Q_0$ and $f_{\mathrm{i}} = f_0$ for the cavity without a sample, but with a sapphire rod inside.

By varying the frequency f_{sw} of the microwave synthesizer and measuring the voltage across the diode, we plotted the microwave power transferred over the cavity as a function of frequency, which was described by the conventional resonance formula

$$P(f_{\mathrm{sw}}) = \frac{P_0}{4(f_{\mathrm{sw}} - f_{\mathrm{i}})^2/f_{\mathrm{i}}^2 + 1/Q_{\mathrm{iL}}^2}\,, \tag{5}$$

where P_0 is a constant independent of the frequency f_{sw}. The resonance frequency f_{i} of the cavity was defined by the peak position on the curve of $P(f_{\mathrm{sw}})$, while the Q-factor of the resonance system was derived from the full bandwidth at half power of the transmission curve $0.5P(f_{\mathrm{i}})$ using $Q_{\mathrm{iL}} = f_{\mathrm{i}}/\delta f_{\mathrm{i}}$, where δf_{i} is a transmission bandwidth. A Q-factor of about 10^7 was measured to within 1%, and the resonance frequency error was within 10 Hz.

2.3 Measured quantities and samples

Figure 5 shows the recorded temperature dependences of the $Q_0(T)$-factor and resonance frequency shift $\Delta f_0(T)$ for an empty cavity as well as for the cavity containing a YBCO single crystal $(Q, \Delta f)$. The Q_0-factor (open squares) is practically independent of temperature, while the pronounced monotone change in Δf_0 (open circles) is due to the temperature dependence of the dielectric constant and thermal expansion of the sapphire rod. The data depicted in Fig. 5 correspond to the measurements carried out on a thick rod of diameter 3.5 mm. The use of a thin rod (2 mm in diameter) leads to a decrease in the shift $\Delta f_0(T)$ by an order of magnitude over the temperature range $4.2 \leqslant T \leqslant 120$ K.

To find a relation between the components $R_{\mathrm{s}}(T)$, $X_{\mathrm{s}}(T)$ of the surface impedance and the measured quantities $Q_{\mathrm{i}}(T)$ and $\Delta\omega_{\mathrm{i}}(T) = 2\pi\Delta f_{\mathrm{i}}(T)$, let us introduce the geometrical factor Γ_{s} of the sample. The difference in the average energy losses pertaining to the cavity with the sample inside and the

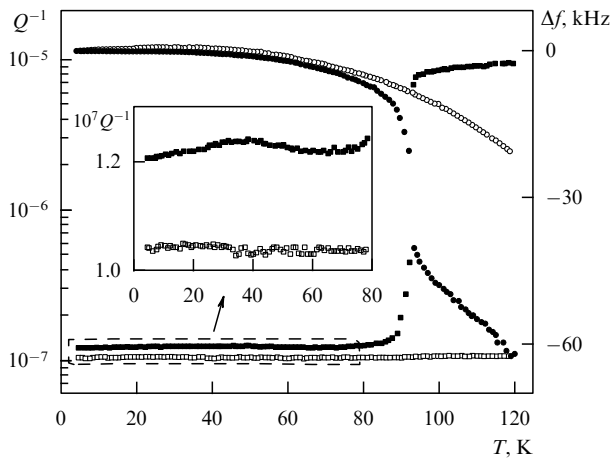

Figure 5. Temperature dependences of $1/Q$ and Δf measured in a YBCO single crystal. The full symbols correspond to the cavity with the sample inside, the open symbols depict data for the empty cavity. The inset shows low-temperature sections of the curve $1/Q(T)$.

empty cavity is equal to the power directly absorbed by the sample:

$$P = \frac{1}{2}\int_S R_s H_s^2 \, dS , \tag{6}$$

where H_s is the tangential component of the microwave magnetic field on the sample surface. In Eqn (6) we integrate over the whole sample surface S. The energy stored in the cavity is equal to

$$W = \frac{\mu_0}{2}\int_V H^2 \, dV , \tag{7}$$

where V is the cavity volume, and H^2 is the squared total magnetic field strength in the cavity with the sample inside. The difference between the reciprocal Q-factors of the cavity is given by

$$\frac{1}{Q} - \frac{1}{Q_0} = \frac{P}{\omega W} = \frac{R_s \int_S H_s^2 \, dS}{\omega\mu_0 \int_V H^2 \, dV} = \frac{R_s}{\Gamma_s} , \tag{8}$$

where

$$\Gamma_s = \frac{\omega\mu_0 \int_V H^2 \, dV}{\int_S H_s^2 \, dS} . \tag{9}$$

Let the complex resonance frequency be $\hat{\omega}$ for the cavity with the sample inside, and $\hat{\omega}_0$ for the empty cavity at the same temperature. The difference $\hat{\omega} - \hat{\omega}_0$ determines the frequency shift caused by the sample, $\hat{\omega}_s$. At the same coupling Q-factors Q_1 and Q_2 we find from Eqns (3), (4), and (8) the quantity $\hat{\omega}_s$:

$$\hat{\omega}_s = \omega_s + \frac{i\omega R_s}{2\Gamma_s} . \tag{10}$$

The change in the sample temperature leading to a change in its impedance $\Delta Z_s(T) = \Delta R_s(T) + i\Delta X_s(T)$ can be considered as a small perturbation resulting in the frequency shift $\Delta\hat{\omega}_s(T)$ in the complex frequency $\hat{\omega} = \hat{\omega}(Z_s)$:

$$\Delta\hat{\omega}_s(T) = \frac{\partial\hat{\omega}}{\partial Z_s}\,\Delta Z_s = \frac{\partial\hat{\omega}}{\partial Z_s}(\Delta R_s + i\Delta X_s) . \tag{11}$$

On the other hand, according to Eqn (10) we have

$$\Delta\hat{\omega}_s(T) = \frac{i\omega}{2\Gamma_s}\left(\Delta R_s - \frac{2i\Gamma_s\Delta\omega_s(T)}{\omega}\right) , \tag{12}$$

then comparing formulae (11) and (12), we find the variation of the surface sample reactance

$$\Delta X_s(T) = -\frac{2\Gamma_s\Delta\omega_s(T)}{\omega} , \tag{13}$$

where $\Delta\omega_s(T) = \Delta\omega(T) - \Delta\omega_0(T)$.

Thus, the temperature dependences of the real and imaginary parts of the surface impedance are derived from the measured curves of $Q_i(T)$ and $\Delta f_i(T)$ with the use of the relations

$$R_s(T) = \Gamma_s\left[Q^{-1}(T) - Q_0^{-1}(T)\right] ,$$

$$X_s(T) = -\frac{2\Gamma_s}{f_0}\left[\Delta f(T) - \Delta f_0(T)\right] + X_0 , \tag{14}$$

where Γ_s is the sample geometrical factor determined by Eqn (9), and X_0 is an additive constant.

The parameter X_0 was found by equating the real and imaginary parts of the impedance for the sample in the normal state, $R_s(T_c) = X_s(T_c)$, since all the samples studied satisfied the conditions of the normal skin-effect. The temperature dependences $R_s(T)$ and $X_s(T)$ coincided at $T \geqslant T_c$. The problem of calculating the geometrical factor Γ_s depending on the sample shape can be solved in the general case only by numerical methods.

The TBCCO and YBCO crystals grown by the methods described in Refs [24, 25] were shaped as plates with characteristic dimensions of $a \times b \times c = 1 \times 1 \times 0.1$ mm^3 (TBCCO) and $1.5 \times 1.5 \times 0.1$ mm^3 (YBCO). The sample was fixed on the end of the sapphire rod so that the crystal **c**-axis was aligned with the microwave magnetic field, $\mathbf{H}_0 \| \mathbf{c}$. In this case, high-frequency currents circulate in the *ab* plane of the crystals and their geometrical factors can be estimated using Eqn (9) on the assumption that the magnetic field strength on the sample surface is equal to the field amplitude H_0 at the centre of the empty cavity:

$$\Gamma_s = \frac{\omega\mu_0 V}{4\gamma_0 A} , \qquad \gamma_0 = \frac{V H_0^2}{2\int_V H^2 \, dV} , \tag{15}$$

where A is the area of the *ab* face of the sample, and γ_0 is a constant determined by the field distribution for the H_{011} mode [26]. With regard to the size of our cavity we have $\gamma_0 = 5.3$. The geometrical factor Γ_s of one such sample was calculated using Eqn (14) with the measured values of $Q(T_c)$ and the resistivity $\rho(T_c) = 2R_s^2(T_c)/\omega\mu_0$. This experimental value of Γ_s was 60% lower than that calculated without regard for the demagnetization factor in expression (15). Below we shall take into account this correction to calculations of the geometrical factor for YBCO and TBCCO crystals when determining the absolute values of the impedance $Z_s(T)$. Figure 6 shows the dependences $R_s(T)$ and $X_s(T)$ for the YBCO single crystal, where $\Gamma_s = 1.76 \times 10^4$ Ω. They were calculated using Eqn (14) with the use of the measured data on $1/Q_i(T)$ and $\Delta f_i(T)$ plotted in Fig. 5.

The BKBO crystals were prepared by electrochemical crystallization [27, 28] and took on a cubelike form. We investigated different samples with volumes varying from 0.2 to 1.5 mm^3. The geometrical factor was evaluated as

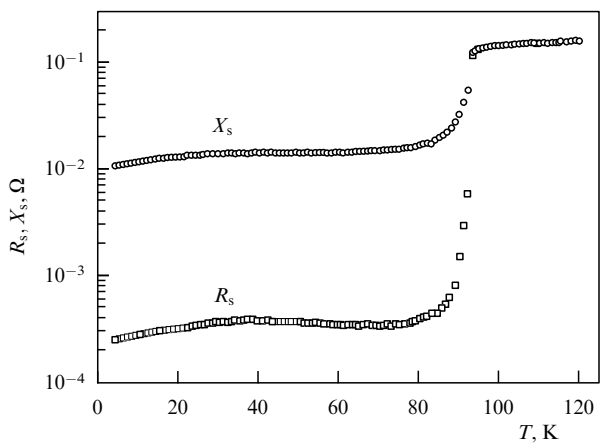

Figure 6. Surface resistance R_s and reactance X_s of a YBCO single crystal as functions of temperature.

follows. We fabricated a niobium sample whose size and shape were the same as those of the BKBO sample studied. If the samples were ellipsoids, then the geometrical factors Γ_{BKBO} and Γ_{Nb} were calculated exactly.

For example, the geometrical factor for a spheroid shaped sample of radius r, located at the centre of a cavity operating at the H_{011} mode [29], is equal to $\Gamma_{\mathrm{s}} = \omega\mu_0 V/12\pi\gamma_0 r^2$. Therefore, our first step was to evaluate $\Gamma_{1,\mathrm{Nb}}$ and $\Gamma_{1,\mathrm{BKBO}}$ for the samples under the assumption that both the samples are spheroids having volumes equal to the known volumes of the Nb and BKBO samples. The second step was based on the experimental method for determining Γ_{Nb}. We measured the resistivity $\rho_{\mathrm{Nb}}(10\ \mathrm{K})$ of a thin strip of Nb cut from the same material as the niobium sample itself and calculated the surface resistance $R_{\mathrm{s}}(10\ \mathrm{K})$ using the formula for the normal skin effect. Then, substituting this value and the measured value of $Q_{\mathrm{i,Nb}}(T)$ into Eqn (14), we found the geometrical factor. The estimated value of Γ_{Nb} was only 24% smaller than the value of $\Gamma_{1,\mathrm{Nb}}$ calculated by the first method. Taking into account the similarity between the shapes of the Nb and BKBO samples investigated, we set the geometrical factor of the BKBO crystals equal to $\Gamma_{\mathrm{BKBO}} = 0.76 \times \Gamma_{1,\mathrm{BKBO}}$. Figure 7 depicts the experimental dependences $R_{\mathrm{s}}(T)$ and $X_{\mathrm{s}}(T)$ for a BKBO single crystal whose geometrical factor was $\Gamma_{\mathrm{s}} = 3.3 \times 10^4\ \Omega$.

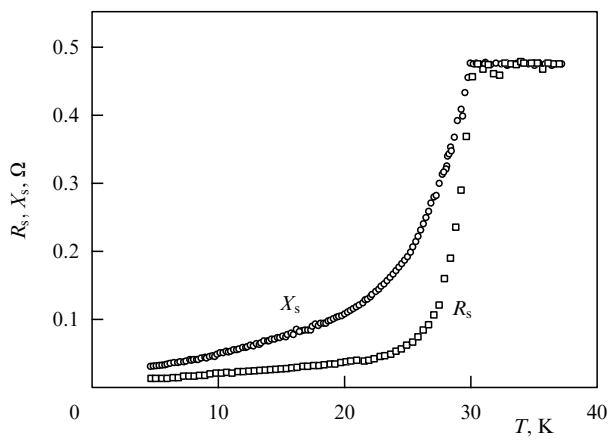

Figure 7. Temperature dependences of the surface resistance R_{s} and reactance X_{s} in a BKBO single crystal.

2.4 Factors affecting the accuracy of measurements

Considering the technique for measuring the Q-factor and the resonance frequency shift and calculating the absolute values of the impedance components, we should discuss factors determining the accuracy of the measurements. The factors can be divided into two groups, i.e. those which are experimentally controlled and those which are not controlled and result from uncertainty introduced by the sample.

The first group includes the following effects.

1. Evacuation of the cavity unit. When the sample is heated, the flux of residual heat-transfer gas in the region between the sapphire rod and the cavity lids elicits a temperature gradient along the sample holder. The gradients are negligible if the cavity pressure does not exceed 10^{-3} mm Hg. In the experiments with single-crystal YBCO samples, for example, a cavity pressure exceeding this value several times enhanced the measured transition temperature T_{c} by several degrees.

2. External pressure. A 1 mm Hg change in the helium pressure in the cryostat was found to lead to a rather large shift of the resonance frequency by $\simeq 0.7$ kHz, which is particularly essential in measurements of $\Delta f(T)$ over the region of low temperatures. Therefore in the experiment we stabilized the helium pressure to an accuracy of 0.02 mm Hg.

3. Thermal cycling. Upon completing the impedance measurements as a function of temperature on the sample in both the superconducting and normal states, we must necessarily measure parameters of the empty cavity at the same temperatures. Carrying out all the experiments we should ensure that the positions of the sapphire rod and waveguide – cavity coupling loops are reproduced, the influence of these loops on the measured values of $Q_{\mathrm{i}}(T)$ and $\Delta f_{\mathrm{i}}(T)$ exactly controlled, the level of liquid helium in a cryostat fixed in all experiments, and, finally, the electronic circuit operated with a high stability.

The above effects are the main 'external' factors influencing the accuracy of measurements. They are obviated if we carefully control the experimental conditions. However, there are some uncontrollable 'intrinsic' effects which may also be significant.

1. Field distribution over the sample surface and the geometrical factor Γ_{s}. According to Eqn (9), to calculate Γ_{s} we should take an integral $\int_S H_{\mathrm{s}}^2\,\mathrm{d}S$ over the sample surface. For a sample with the shape of a thin square slab with characteristic dimensions $a \cdot a \cdot c$, $c \ll a$, the integral is equal to $2H_0^2 a^2(1 + 2c/a)$, assuming that the tangential component H_{s} of the magnetic field strength on the sample surface is coincident with the field amplitude H_0 at the centre of the cavity. With an accuracy of magnitude $c/a \ll 1$, the above relation is in agreement with formula (15) determining the factor Γ_{s}. It is obvious, however, that the approximation $H_{\mathrm{s}} \approx H_0$ is valid if the ab-plane of the slab is parallel to the field $\mathbf{H}_0$ and the demagnetization factor of the sample is very small. If the field $\mathbf{H}_0$ is perpendicular to the slab, $\mathbf{H}_0 \| \mathbf{c}$, and the measurements are made of microwave crystal characteristics pertaining to the ab-plane, it is not surprising that the increased demagnetization factor results in a significant difference between the value of Γ_{s} calculated using Eqn (15) and that established experimentally. In this connection an attempt to approximate to the sample with a flattened ellipsoid of revolution with semiaxes $c/2$, $a/2$ and a certain field distribution H_{s} over the sample surface [30 – 32] is also not correct, since the edge field $H_{\mathrm{edge}} = 2\pi a H_0/c$ of the ellipsoid far exceeds the actual value. It is more suitable to approximate the sample shape by a slab with slightly rounded edges [33]. This approach yields the well-known geometrical barrier to penetration of flux lines from the sample edges [33 – 35]. In this case, the field distribution over the sample surface in the Meissner state† is given by the formula [33]

$$H_{\mathrm{s}}(x) = \frac{H_0 x}{\sqrt{(a/2)^2 - x^2}}\,, \qquad -\frac{a}{2} + \frac{c}{4} \leqslant x \leqslant \frac{a}{2} - \frac{c}{4}\,,$$

except for a very narrow region ($\approx c/4$) near the edges, where $\int_S H_{\mathrm{s}}^2\,\mathrm{d}S$ is logarithmically divergent. The field is assumed to be homogeneous and equal to $H_{\mathrm{edge}} \approx H_0\sqrt{a/c}$ on the lateral

† At $T < T_{\mathrm{c}}$, the high-frequency field penetrates the sample to the depth $\lambda \sim 10^{-4}$ mm, while at $T \geqslant T_{\mathrm{c}}$ to the skin depth $\delta = \sqrt{2\rho/\omega\mu_0}$ equal to $\sim 5 \times 10^{-3}$ mm at a frequency of ~ 10 GHz and resistivity $\rho(T_{\mathrm{c}}) \sim 100\ \mu\Omega$ cm typical of HTSC crystals. Since the thickness of the crystals studied was about $c \approx 10^{-1}$ mm and $\lambda \ll c$, $\delta \ll c$, the distribution of the field H_{s} and therefore the value of Γ_{s} are practically unchanged with temperature.

faces of the crystal. At $c \ll a$, the integral

$$\int_S H_s^2 \, dS = 16 \int_0^{(a-c/2)/2} H_s^2(x) x \, dx + 4acH_0^2 \frac{a}{c}$$
$$\simeq 2H_0^2 a^2 \left(\ln\left(\frac{a}{c}\right) + 1 \right) \tag{16}$$

exceeds the value of $2H_0^2 a^2$ used in Eqn (15) by a factor of $\left[\ln(a/c) + 1\right]$. Then the geometrical factor Γ_s calculated from Eqns (9) and (16) is less by the same factor. In YBCO single crystals $a/c \approx 15$ and the geometrical factor decreases approximately by 60%, which is in agreement with the experimental value.

2. Thermal expansion of the sample. This is an uncontrollable source of possible errors in measuring the dependence $\lambda(T)$. Changes Δl_i (Δa and Δc) in the sizes of the sample $a \cdot a \cdot c$, $c \ll a$ under thermal cycling, which correspond to a change in the sample volume by $(\Delta c \cdot a^2 + 2\Delta a \cdot ac)$, lead to a parasitic shift in the resonance frequency of the cavity by

$$\Delta f_l(T) = \frac{f_0 \mu_0}{4W} \int_S \Delta l_i(T) H_s^2 \, dS, \tag{17}$$

where W is determined by formula (7). Strictly speaking, the quantity $\Delta f_l(T)$ together with $\Delta f_0(T)$ should be taken into account in expression (14) to calculate $X_s(T)$. Let us estimate this contribution by comparing expression (17) with the resonance frequency shift caused by the change $\Delta\lambda(T)$ in the field penetration depth:

$$\Delta f_\lambda(T) = \frac{f_0 \mu_0}{4W} \int_S \Delta\lambda(T) H_s^2 \, dS. \tag{18}$$

If the ab-plane of the crystal (in our case $a \approx b$) is perpendicular to the magnetic field (transverse orientation) in the measurements of $\Delta\lambda_{ab}(T)$, then using relations (16)–(18) we easily find that

$$\frac{\Delta f_l}{\Delta f_\lambda} = \frac{\Delta c/2\left(\ln(a/c) - 1\right) + \Delta a}{\Delta\lambda_{ab}\left(\ln(a/c) + 1\right)}, \tag{19}$$

i.e. the ratio is equal to $\Delta f_l / \Delta f_\lambda \simeq 0.25(\Delta c + \Delta a)/\Delta\lambda_{ab}$ for the appropriate values of a/c.

In YBCO and BSCCO single crystals with $T_c \simeq 90$ K, the value of λ_{ab} increases by approximately a thousand ångström when the temperature varies from 4.2 to 80 K and many-fold greater at higher temperatures. According to the experimental data, a relative change in the sample sizes $\varepsilon_i = \Delta l_i / l_i$ is very small, $\varepsilon_i < 10^{-5}$, for YBCO [36–38] and BSCCO [39, 40] crystals at $T < 30$ K. In the temperature range $30 < T < 100$ K, the thermal expansion coefficients $\alpha_i = d\varepsilon_i/dT$ are approximately linear functions of temperature: $\alpha_{ab} \approx 0.3 \times 10^{-7} T$ in the ab-plane and $\alpha_c \approx 10^{-7} T$ in the c direction of the YBCO crystal. Therefore we find $\varepsilon_{ab} \approx 10^{-4}$, $\varepsilon_c \approx 3 \times 10^{-4}$, and for typical sample dimensions $a \approx b \approx 1$ mm and $c \approx 0.1$ mm they increase by $\Delta a \approx \Delta b \approx 1000$ A and $\Delta c \approx 300$ A on heating from 30 to 100 K.

In the single-crystal BSCCO, ε_{ab} is twice as large and ε_c is approximately the same as in YBCO crystals. The relative change in the dimensions of BKBO single crystals is rather small over the temperature range $0 < T \leqslant 2T_c$: $\varepsilon < 10^{-5}$ [41]. We are unacquainted with data on the thermal expansion of TBCO and TBCCO crystals at temperatures $T \leqslant T_c$.

Thus, the contribution of $\Delta f_l(T)$ to the total frequency shift of the cavity with a sample (YBCO or BSCCO) inside is negligible in the low-temperature range. However, at intermediate temperatures it may be quite considerable, although less than $\Delta f_\lambda(T)$ in accordance with Eqn (19). This fact should be taken into account when using formula (14) to determine $\lambda_{ab}(T)$. Since the thermal expansion of samples is not controlled in the microwave experiments, the only test of reliability for the experimental curves $\lambda_{ab}(T)$ is that they should be reproduced for crystals of various sizes.

Let us also estimate the factor $\Delta f_l(T)$ if the field $\mathbf{H}_0$ is parallel to the ab plane of the crystal (longitudinal orientation). In this case the tangential component of the magnetic field H_s on the sample surface can be considered equal to H_0, $H_s \approx H_0$. High-frequency currents circulate across all the crystal faces, hence they all contribute to the measured effective magnitude of the impedance. The currents running across the ab planes penetrate the sample to the depth λ_{ab}, while the currents along the c direction penetrate to the depth λ_c, whereas in the experiments we measure an effective depth λ_{eff}. From formula (18) we easily find the relationship between variations of these values†:

$$\Delta\lambda_c = \frac{1}{c}\left[(a + 2c)\Delta\lambda_{eff} - (a + c)\Delta\lambda_{ab}\right]. \tag{20}$$

Using (17) and (18) for $c/a \ll 1$, we arrive at

$$\frac{\Delta f_l}{\Delta f_\lambda} \simeq \frac{\Delta c(1 + 2\varepsilon_{ab}/\varepsilon_c)}{2\Delta\lambda_{eff}}. \tag{21}$$

According to (21), for the longitudinal orientation of the crystal the thermal expansion can introduce distortions $\sim \Delta c$ to the dependence $\lambda_{eff}(T)$ calculated using (14).

3. Data on the surface impedance and complex conductivity measured in YBCO, BSCCO, TBCCO, TBCO, and BKBO single crystals: some distinctive and common features

Microwave measurements of the surface impedance of HTSCs have been performed since the discovery of high-T_c crystals in 1986–1987. The first studies of ceramics as well as superconducting films and crystals fabricated a short time later were fragmentary and qualitative, since the quality of the samples left much to be desired. Particularly, the residual surface resistance $R_{res} = R_s(T \to 0)$ exceeded that of conventional superconductors based on Nb and Pb compounds by several orders of magnitude, and everybody understood that the high-frequency properties of HTSC samples were mainly determined by crystal imperfections due to the structure's inhomogeneity, weak links, twins and other defects in the surface layer. Perhaps the only reliable experimental fact at that time was the proof of the absence of a coherent peak in microwave conductivity $\sigma_1(T)$, i.e. instead of a wide peak in the region $T \sim 0.85T_c$, as follows from the BCS model (see Fig. 1), a narrow peak in $\sigma_1(T)$ was observed near T_c, the peak width virtually coinciding with the width of the phase transition from the normal state to the superconducting one, which was detected in the curve $R_s(T)$.

The situation changed drastically in 1992–1993 when the first high-quality YBCO single crystals [19–21] and thin

† Measuring the crystal $\lambda_{ab}(T)$ for the transverse and $\lambda_{eff}(T)$ for the longitudinal orientations, one can determine the temperature dependence $\lambda_c(T)$ using (20).

films [42] with substantially decreased resistance R_{res} were fabricated. The measurements carried out on these samples revealed silent features of the low-temperature surface impedance $Z_s(T)$, which had not been observed earlier because of great residual losses. It has taken two more years to confirm these peculiarities (first discovered by the UBC group) in YBCO single crystals. Experiments using centimeter waves and the method described in the previous section were carried out in Maryland University [43], Northeastern University (NEU) (Boston) [44], and Tokyo University [45]. The summary result of the experiments was the following:

(a) the linear dependences $\lambda_{ab}(T)$ and $R_s(T)$ are observable for $5 < T < 30$ K;

(b) there is a wide peak in $R_s(T)$ centred at 40 K.

Notice that the above properties of the impedance $Z_s(T)$ are only characteristic of the most perfect YBCO crystals. As was shown in Refs [46–48], the introduction of Zn impurities to perfect single crystals changed the linear dependence of $\lambda_{ab}(T)$ to quadratic and 'smoothed out' the peak in $R_s(T)$. The quadratic dependence $\Delta\lambda_{ab}(T) \propto T^2$ is typical of YBCO thin films [49–51], where the presence of impurities and weak links is more probable than in single crystals. Therefore, it is believed that the T^2-dependence of $\lambda(T)$ is governed by the 'defectiveness' of the samples (extrinsic origin) to a greater extent than the peculiarities (a) and (b) conforming to the internal microscopic properties of the crystals (intrinsic behaviour). Later on this conclusion was confirmed by detailed studies of YBCO films [52], where the quadratic temperature dependence of $\lambda(T)$ became linear at low temperatures as the quality of films increased.

A comprehensive analysis of the data obtained by microwave measurements in YBCO crystals and films through 1996 is given in Ref. [53], and we do not intend to repeat it here. A pronounced difference in the temperature dependences of the surface impedance of YBCO single crystals and conventional superconductors raised the reasonable question of whether the above peculiarities (a) and (b) are typical of other HTSC compounds, which are in contrast to YBCO samples having a tetragonal structure and not containing CuO-chains or copper atoms at all. In the past two-three years, significant technological progress has been achieved in the fabrication of HTSC samples, which has enabled the investigation of the microwave properties of high-quality BSCCO [54–56], BKBO [28], TBCCO [57], and TBCO [58] single crystals. Furthermore, a marked decrease in the times required for the technique to homogenize the growth solution and grow single crystals from standard zirconium dioxide (ZrO_2) crucibles stabilized by yttrium [19] and from other crucibles ($BaZrO_3$) [59] has allowed the fabrication of high-quality YBCO single crystals with resistivity $\rho(T_c) < 40$ μΩ cm which is less than that reported earlier. Microwave measurements on crystals grown by the accelerated technique from ZrO_2 crucibles and from new $BaZrO_3$ crucibles have recently been carried out at the Institute of Solid-State Physics (ISSP, Chernogolovka) [25, 57] and by the research group at NEU (Boston) [60, 61]. These studies detected the above peculiarities of $\lambda_{ab}(T)$ and $R_s(T)$ observed earlier at low temperatures [20, 21, 43–45, 48] as well as some new features of the curves $Z_s(T)$ at higher temperatures.

Figure 6 plots experimental results on the surface resistance $R_s(T)$ and reactance $X_s(T)$ measured at a frequency of ≈ 10 GHz in a YBCO single crystal, while Figs 7 and 8 show similar dependences for BKBO and BSCCO samples, respectively. For $T \geqslant T_c$, these results are equal $[R_s(T) = X_s(T)]$ for all the figures, corresponding to the condition of the normal skin-effect. The values of $X_s(T)$ are calculated with formula (14), the additive constant X_0 being found by matching the temperature dependences $\Delta X_s(T)$ and $\Delta R_s(T)$ for $T \geqslant T_c$. The dependence $X_s(T)$ derived from the data of absolute measurements in turn determines the magnitude of $\lambda(0) = X_s(0)/\omega\mu_0$. Using the experimental value of $R_s(T_c) = \sqrt{\omega\mu_0\rho(T_c)/2} \approx 0.12$ Ω for a YBCO single crystal (see Fig. 6), we find $\rho(T_c) \approx 38$ μΩ cm [25]. All the temperature dependences $R_s(T) = X_s(T)$ depicted in Figs 6, 7, and 8 are well approximated by $2R_s^2(T)/\omega\mu_0 = \rho(T) = \rho_0 + bT$ in the temperature range $T \geqslant T_c$. For example, these parameters are equal to $\rho_0 \approx 11$ μΩ cm and $b \approx 1.4$ μΩ cm/K for the BSCCO single crystal (see Fig. 8) [54].

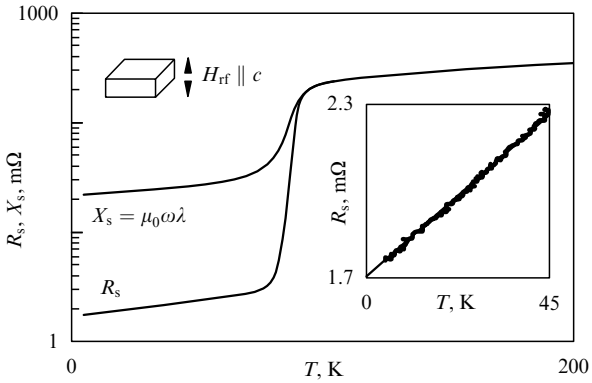

Figure 8. Temperature dependence of the surface impedance $Z_s = R_s + iX_s$ for a BSCCO single crystal in the normal and superconducting states [54]. The inset depicts the low-temperature $R_s(T)$.

For various HTSC single crystals in the superconducting state it is convenient to compare the temperature dependences $Z_s(T)$ by dividing the temperature interval of interest into three parts: low temperatures ($T < T_c/3$), intermediate temperatures ($T \sim T_c/2$), and temperatures near the transition point T_c.

3.1 Low temperatures: $T < T_c/3$

Figure 9 plots the typical dependences $R_s(T)$ and $\lambda(T)$ at $T < 0.7T_c$ for YBCO [25], TBCCO [57], and BKBO [28] single crystals fabricated at the ISSP. The dependences measured on the YBCO and BKBO samples correspond to the low-temperature portions of the curves depicted in Figs 6 and 7.

The variation of surface resistance $\Delta R_s(T) \propto T$ is revealed at low temperatures in all the crystals (Fig. 9). A similar linear dependence $\Delta R_s(T)$ occurs in BSCCO single crystals (see the inset to Fig. 8) and TBCO single crystals [58].

The dependences $\Delta\lambda(T) = \Delta X_s(T)/\omega\mu_0$ are also linear for YBCO (Fig. 9), BSCCO (Figs 8 and 10), and TBCO (Fig. 11) single crystals at $T < T_c/3$. The curves $\lambda(T)$ (Fig. 9) demonstrate clearly defined linear dependences for the TBCCO sample at $T > 12$ K and the BKBO sample at $T > 5$ K.

By extrapolating the low-temperature portions of curves $\lambda(T)$ (Fig. 9) and $X_s(T) = \omega\mu_0\lambda(T)$ (Fig. 8) to the limit $T = 0$, we find the following values of $\lambda_{ab}(0)$ for various single crystals: 1400 A (YBCO), 3700 A (TBCCO), 3000 A (BKBO), and 2600 A (BSCCO).

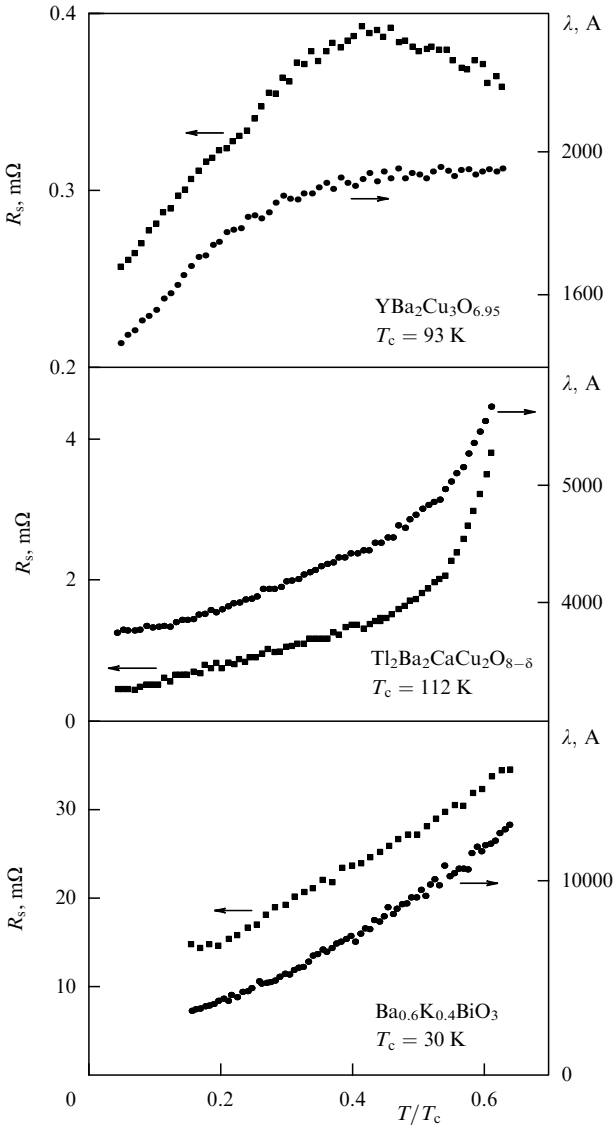

Figure 9. Surface resistance R_s and penetration depth λ of YBCO, TBCCO, and BKBO single crystals as functions of temperature for $T < 0.7T_c$.

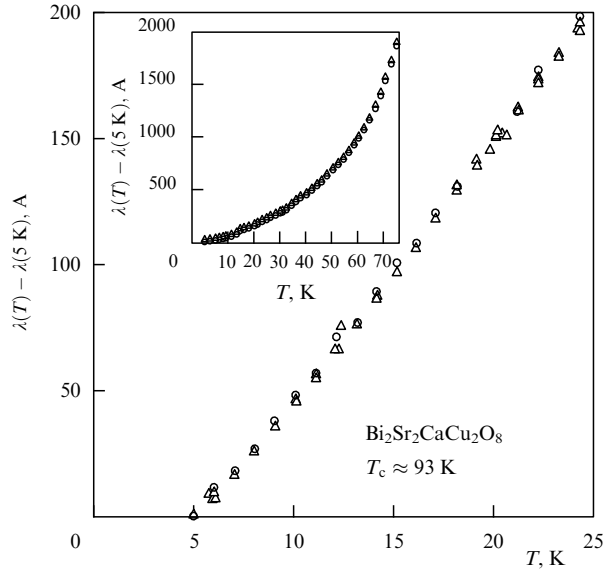

Figure 10. Linear variation of the low-temperature penetration depth $\Delta\lambda(T)$ in a BSCCO single crystal [56]. The inset shows the dependence $\Delta\lambda(T)$ over the whole temperature range.

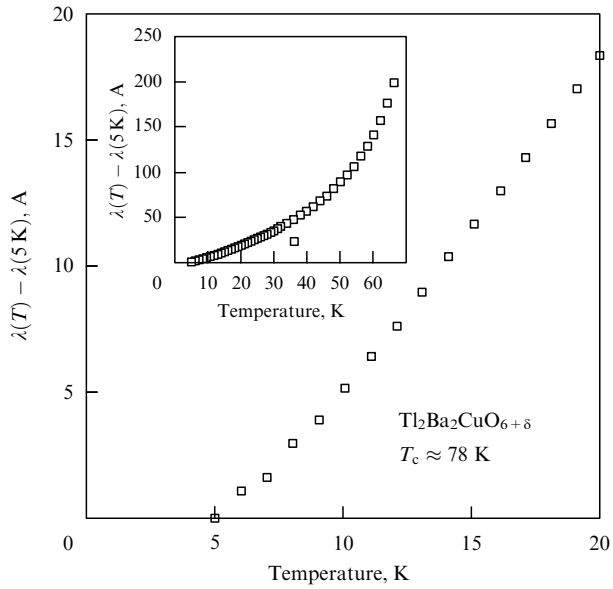

Figure 11. Linear variation of the low-temperature penetration depth $\Delta\lambda(T)$ in a TBCO single crystal [58]. The inset shows the dependence $\Delta\lambda(T)$ over a wide temperature range.

3.2 Intermediate temperatures: $T \sim T_c/2$

At frequencies near ~ 10 GHz, the linear dependence $\Delta R_s(T) \propto T$ extends up to temperatures $\sim T_c/2$ in BSCCO (Fig. 8), TBCCO, BKBO (Fig. 9), and TBCO [58] single crystals. The penetration depth $\lambda(T)$ of the crystals monotonically increases as the temperature rises.

The general behaviour of the surface impedance of HTSC single crystals with a tetragonal structure breaks down in YBCO crystals. As was emphasized above all the microwave measurements on high-quality YBCO single crystals demonstrate a wide peak of $R_s(T)$ centred at $T \sim 40$ K (see Figs 5, 6, and 9). The main origin of the difference between YBCO and other HTSC single crystals remains to be seen. It is unlikely that the absence of the peak in the crystals with tetragonal structure is associated with the insufficient quality of the crystals, as with YBCO crystals doped with Zn impurities [46–48]. Apart from a body of evidence of the monotone dependence $R_s(T)$ in BSCCO, TBCO, TBCCO, and BKBO crystals, a similar peak was observed in such YBCO crystals [44, 45, 57], where the parameters R_{res} and $\rho(T_c)$ characterizing the sample quality were lower than in BSCCO [56] and TBCCO [57] samples. Most likely, the origin of the effect is the CuO chains introduced only into the orthorhombic structure of YBCO samples. The electrons of the chains form an additional band, contributing to the observed dependence $Z_s(T)$. This contribution seems to result in another peculiarity typical of only YBCO samples, i.e. a plateau (Fig. 9) or bump (Fig. 12) in the curve $\lambda_{ab}(T)$.

So far this peculiarity has been observed only in the most perfect YBCO single crystals [25, 57, 60, 61] and thin films [42, 62]. Curve *1* in Fig. 12 corresponds to a YBCO single crystal, whose $\rho(T_c)$ and R_{res} are really less than that in samples *2* and *3* revealing the typical temperature dependences $\Delta\lambda_{ab}(T)$. The quantities X_s and λ_{ab} in Figs 6 and 9 are almost constant over

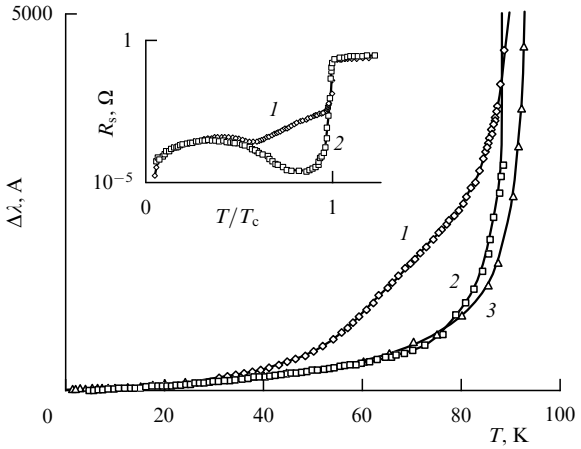

Figure 12. Temperature dependences of the penetration depth $\Delta\lambda$ in YBCO single crystals fabricated in various ways [60]: *1* — using $BaZrO_3$ crucibles; *2* — using ZrO_2 crucibles doped with yttrium; curve *3* corresponds to data of Ref. [20]. The inset shows the temperature dependences of the surface resistance $R_s(T)$ for the crystals *1* and *2*.

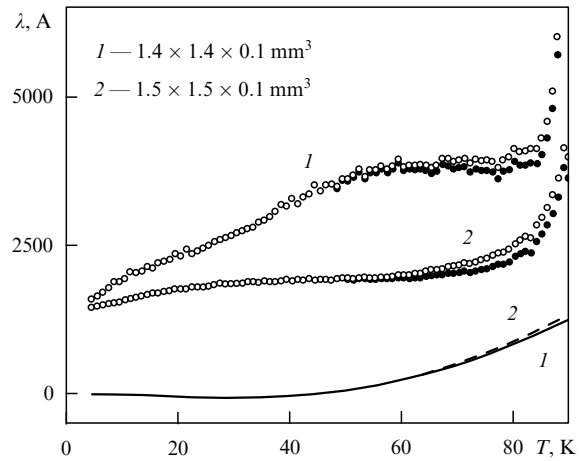

Figure 13. Influence of thermal expansion of the sample on the penetration depth λ_{ab} for two YBCO single crystals.

the temperature range $35 < T < 65$ K. We observed a plateau of approximately similar width ~ 20 K in the $\lambda_{ab}(T)$ curves for several YBCO single crystals fabricated by the same method [25], but the positions of these plateaus were different with respect to $T_c/2$. For example, the plateau in the $Z_s(T)$ curve was shifted to higher temperatures $60 < T < 85$ K for a sample used in Ref. [57], whose surface was less than that used in Ref. [25] (see Figs 6 and 9).

Features of the imaginary part of the surface impedance $X_s(T)$ at intermediate temperatures should be considered carefully, since the $\lambda(T)$ curves may be distorted due to thermal expansion of the crystal. With regard to this effect, the difference $\Delta f_{exp}(T) = \Delta f(T) - \Delta f_0(T)$ in formula (14) found by the successive measurements in the cavity with and without the sample inside should be written as $\Delta f_{exp}(T) = \Delta f_\lambda(T) - \Delta f_l(T)$, where $\Delta f_\lambda(T)$ and $\Delta f_l(T)$ are the resonance frequency shifts caused by changes in the penetration depth and sample sizes due to thermal expansion. When the sample is in the transverse orientation with respect to the field $\mathbf{H}_0$, the ratio $\Delta f_l/\Delta f_\lambda$ can be estimated using formula (19). We now compare the curves $\Delta\lambda_{exp}(T) \propto [\Delta f(T) - \Delta f_0(T)]$ measured in YBCO crystals of sizes $a \approx b \approx 1.4$ mm, $c \approx 0.1$ mm [57], and $a \approx b \approx 1.5$ mm, $c \approx 0.1$ mm [25] with the dependences $\Delta\lambda(T) \propto [\Delta f_{exp}(T) + \Delta f_l(T)]$ accounting for the contribution $\Delta f_l(T)$. Figure 13 demonstrates the temperature dependences (the low solid line *1* and low dashed line *2* at the bottom of the figure) of the numerator in the right-hand side of Eqn (19) for two YBCO crystals with parameters a and c given above. The experimental values

$$\Delta c(T) = c\int \alpha_c(T)\,\mathrm{d}T \quad \text{and} \quad \Delta a(T) = \frac{a}{2}\int \left[\alpha_a(T) + \alpha_b(T)\right]\mathrm{d}T$$

were taken from Ref. [38]; the closed circles (λ_{exp}) correspond to the data of Refs [57] (curve *1*) and [25] (curve *2*), while the open circles (λ) take into account the corrections caused by thermal expansion of crystals and calculated by Eqn (19). For $T < 50$ K, the dependences $\lambda_{exp}(T)$ and $\lambda(T)$ coincide, while they differ a little at higher temperatures. Therefore we may conclude that the plateaus in the $\lambda(T)$ curves, detected in Refs [25] and [57], are the real features of the surface reactance $X_s(T)$ of YBCO single crystals at intermediate temperatures. But the temperature dependences of the surface resistance $R_s(T)$ observed in these experiments were typical (see Fig. 6).

Finally, we point out one more feature of the surface impedance of high-quality YBCO crystals, namely, the broad peak in the curve $R_s(T)$ centred at $T \sim 40$ K is followed by a substantial increase in resistance; the latter has been observed in recent experiments [60, 61]. The dependence $R_s(T)$ taken from Ref. [60] is depicted in the inset to Fig. 12 (curve *1*). This dependence is easily calculated from formula (14) with the use of the measured data on the Q-factor of the cavity. The thermal expansion of the sample has no effect on the dependence. The YBCO single crystals grown from $BaZrO_3$ crucibles [60, 61] are the most perfect samples containing a single phase†, for which a smooth growth of the dependence $R_s(T)$ in the temperature range $T_c/2 < T < T_c$ is a common feature [61].

3.3 Temperatures near T_c: $T \to T_c$

After a transition to the superconducting state, the surface resistance $R_s(T)$ rapidly drops for all HTSC single crystals. At frequencies about 10 GHz, the resistance R_s of high-quality YBCO crystals drops by a factor of one hundred or more when the temperature decreases by 1 K below T_c. The quantity $X_s(T)$ also sharply decreases near the transition temperature, but more weakly than the surface reactance $R_s(T)$. There is no consensus of opinion regarding the temperature dependence of the penetration depth $\lambda_{ab}(T)$ near the transition temperature. So far this dependence has been studied thoroughly only for high-quality YBCO single crystals grown by various methods. The authors of Refs [63, 12] observed the dependence $\lambda_{ab}(T) \propto (1 - T/T_c)^{-0.33}$ corresponding to the so-called 3D XY fluctuation model [65–67]. The dependence $\lambda_{ab}(T) \propto (1 - T/T_c)^{-0.5}$ consistent with the BCS model was experimentally examined in Ref. [61] near the transition temperature. In YBCO single crystals fabricated at the ISSP, the power index appeared to be intermediate between these values of -0.33 and -0.5.

† A sharp decrease (a jump) in the curve $R_s(T)$ detected by microwave measurements in HTSC crystals at a certain transition temperature T_c may indicate appearance of the superconducting phase at the same temperature T_c, which was observed in the TBCCO crystal [57] with two superconducting phases 2212 ($T_{c1} \simeq 112$ K) and 1212 ($T_{c2} \simeq 81$ K) [64].

3.4 Complex conductivity

Let us consider now the temperature dependences of the complex conductivity $\sigma_s = \sigma_1 - i\sigma_2$. The real $\sigma_1(T)$ and imaginary $\sigma_2(T)$ parts of the conductivity are not directly measured in the experiments, but can be calculated using formula (2) with the use of the measured values of $R_s(T)$ and $X_s(T)$.

In high-quality HTSC crystals $R_s(T) \ll X_s(T)$ and Eqn (2) simplifies at temperatures far from T_c:

$$\sigma_1(T) = \frac{2\omega\mu_0 R_s(T)}{X_s^3(T)}\,, \qquad \sigma_2(T) = \frac{\omega\mu_0}{X_s^2(T)}\,. \tag{22}$$

As a result, the ratio is small: $\sigma_1/\sigma_2 = 2R_s/X_s \ll 1$ at low and intermediate temperatures. The variations $\Delta\sigma_1(T)$ and $\Delta\sigma_2(T)$ are determined by the relative changes $\Delta R_s(T)$ and $\Delta X_s(T)$:

$$\Delta\sigma_1 \propto \left(\frac{\Delta R_s}{R_s} - 3\,\frac{\Delta X_s}{X_s}\right), \qquad \Delta\sigma_2 \propto -\frac{\Delta X_s}{X_s}\,. \tag{23}$$

Thus, the curves $\sigma_2(T)$ are determined only by the function $X_s(T) = \omega\mu_0\lambda(T)$ and reflect the main properties of the temperature dependence of the penetration depth $\lambda(T)$ such as its linearity at low temperatures for all the high-quality HTSC single crystals and the peculiarities observed in YBCO samples at intermediate temperatures. The behaviour of the real part $\sigma_1(T)$ [see Eqn (23)] is determined by the competition of the relative contributions $\Delta R_s/R_s$ and $\Delta X_s/X_s$. In conventional superconductors, for example, Nb, the quantity $X_s(T)$ ($\gg R_s$) is almost fixed ($\Delta X_s \approx 0$) at temperatures $T \leqslant T_c/2$, while the surface resistance $R_s(T)$ decreases exponentially, approaching the constant level of the residual surface resistance R_{res} as $T \to 0$. Subtracting R_{res} from the measured $R_s(T)$, in accordance with Eqns (22) and (23) we arrive at the dependence $\sigma_1(T)$ given by the BCS theory: the real part of the conductivity $\sigma_1 = 0$ at $T = 0$ and increases as a weak exponent at higher temperatures $T \leqslant T_c/2$. The dependences $\sigma_1(T)$ measured in HTSC single crystals significantly differ from those predicted by conventional BCS, SC, and GC models dealing with the microwave response of superconductors. At $T < T_c$, the variations $\Delta R_s(T)$ and $\Delta X_s(T)$ are not small in HTSC samples with $\Delta X_s(T) \gg \Delta R_s(T)$. Therefore, though the inequality $R_s(T) < X_s(T)$ is valid, the increment $\Delta\sigma_1(T)$ in Eqn (23) changes sign from plus to minus as the temperature rises starting from $T = 0$, i.e. the curve $\sigma_1(T)$ passes a maximum, whose position and height depend on the choice of R_s†. Let us extrapolate the curve $R_s(T)$ at $T \ll T_c$ using a linear dependence down to $T = 0$ and propose $R_s(0)$ to be equal to the residual surface resistance, $R_s(0) = R_{res}$. Then, by analogy with conventional superconductors using only the temperature-dependent difference $R_s(T) - R_{res}$ (intrinsic behaviour) for determining $\sigma_1(T)$ in the numerator of Eqn (22), we find that all the required dependences $\sigma_1(T)$ in HTSC single crystals take the form of a wide peak. Starting from the zero value $\sigma_1(0) = 0$, the conductivity $\sigma_1(T)$ sharply increases linearly up to a maximum $\sigma_{1\,max}$, which always greatly exceeds the conductivity $\sigma_1(T_c)$ in the normal state, $\sigma_{1\,max} \gg \sigma_1(T_c)$. In HTSC crystals with a tetragonal structure, the maximum $\sigma_{1\,max}$ occurs at $T_m \approx T_c/3$, while in YBCO samples the temperature of the maximum T_m virtually coincides with that of the dependence $R_s(T)$. In addition, the conductivity curve $\sigma_1(T)$ for these samples also exhibits the above peculiarities of the impedance $Z_s(T)$, observed in YBCO single crystals at intermediate temperatures [25, 57, 60, 61]. Figure 14 plots the dependence $\sigma_1(T)$ measured in a YBCO single crystal, for which the curves $R_s(T)$ and $X_s(T)$ are presented in Figs 6 and 9.

† As a result, strictly speaking the $\sigma_1(T)$ curves are not single-valued at $T \leqslant T_c/2$ in contrast to the experimental dependences $R_s(T)$ and $X_s(T)$.

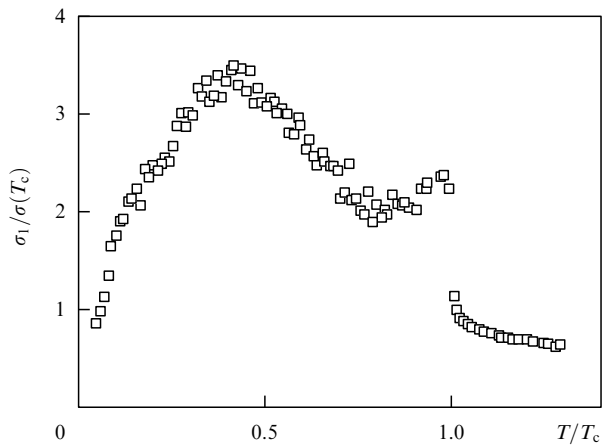

Figure 14. Real part of the conductivity $\sigma_1(T)/\sigma(T_c)$ in a YBCO single crystal, calculated using Eqn (25). The values of $R_s(T)$ were derived from the data depicted in Figs 6 and 9 by subtracting the residual surface resistance $R_{res} \simeq 230\ \mu\Omega$.

Now let us dwell on the trend of the $\sigma_s(T)$ curve near T_c, when Eqns (22) and (23) are not valid. In this temperature range we should use the local relations (1) and (2) or their analogs for normalized quantities, to couple the real and imaginary components of the impedance and conductivity:

$$\frac{R_s(T)}{R_s(T_c)} = \sqrt{\frac{\sigma(T_c)(\varphi^{1/2} - 1)}{\sigma_2\varphi}}\,,$$
$$\frac{X_s(T)}{X_s(T_c)} = \sqrt{\frac{\sigma(T_c)(\varphi^{1/2} + 1)}{\sigma_2\varphi}}\,, \tag{24}$$

$$\frac{\sigma_1(T)}{\sigma(T_c)} = \frac{4R_s^2(T_c)R_sX_s}{(R_s^2 + X_s^2)^2}\,,$$
$$\frac{\sigma_2(T)}{\sigma_2(0)} = \frac{\lambda^2(0)}{\lambda^2(T)} = \frac{X_s^2(0)(X_s^2 - R_s^2)}{(R_s^2 + X_s^2)^2}\,. \tag{25}$$

Here $R_s(T_c) = X_s(T_c)$ and $\sigma(T_c) = \sigma_1(T_c)$ are the impedance and conductivity at $T = T_c$, while $X_s(0)$ and $\sigma_2(0)$ are the same quantities at zero temperature, and $\lambda = (1/\omega\mu_0\sigma_2)^{1/2}$, $\varphi = 1 + (\sigma_1/\sigma_2)^2$. The conductivity $\sigma_2(T)$ along the *ab*-plane of HTSC single crystals quickly vanishes in the normal state. The derivative $(T_c/\sigma_2(0))\mathrm{d}\sigma_2(T)/\mathrm{d}T$ at $T = T_c$ varies from -2 to -4 in different crystals. The real part of the conductivity $\sigma_1(T)$ does not show a coherent peak typical of the BCS theory (see Fig. 1) at $T \sim 0.85T_c$. Usually, a very narrow peak of $\sigma_1(T)$ in HTSC single crystals occurs in the interval $T_c - 1$ K, T_c. As the temperature decreases, the peak immediately transforms into a wide maximum centred at $T < T_c/2$. The maximum is caused by inhomogeneous broadening of the superconducting phase transition [9, 10] and fluctuation effects [11]; it was extensively studied in Ref. [12]. However, in perfect YBCO crystals the typical dependence $\sigma_1(T)$ is distorted at temperatures $T > T_c/2$ (see Fig.14) because of peculiarities of the surface impedance $Z_s(T)$ manifesting themselves in this temperature range.

4. A phenomenological description of the experimental data

The macroscopic properties of conventional superconductors are simply and rather successfully described by the phenomenological theory developed by London and London [68] and the corresponding two-fluid model developed by Gorter and Casimir [15], which proposes a local connection between the current density and the vector potential of the magnetic field. To investigate superconductors in an electromagnetic field of frequency ω, we formulate the GC model as follows. A superconductor is assumed to contain a number of carriers n_s in the superconducting state and a number of carriers n_n in the normal state, with the total concentration of carriers being $n = n_n + n_s$ at an arbitrary temperature below the transition one ($T \leqslant T_c$). The carriers have the same charges e and masses m. The first London's equation describes the motion of superconducting carriers. The normal carriers are affected by an alternating electric field and an averaged 'force of friction' containing the relaxation time τ of normal carriers, the motion of the normal carriers being described by Newton's second law. Solving the equations of motion, we obtain the expressions for the real and imaginary parts of the conductivity $\sigma_s = \sigma_1 - i\sigma_2$:

$$\sigma_1 = \frac{n_n e^2 \tau}{m} \frac{1}{1 + (\omega\tau)^2}, \qquad \sigma_2 = \frac{n_s e^2}{m\omega}\left[1 + \frac{n_n}{n_s}\frac{(\omega\tau)^2}{1 + (\omega\tau)^2}\right]. \quad (26)$$

In the GC model the quantity τ is deemed independent of temperature. It is quite reasonable if the normal carriers in the superconductor are believed to behave as electrons in an ordinary metal: they are scattered by impurities at low temperatures (in conventional superconductors $T_c < 10$ K), the scattering being independent of temperature. Then the temperature dependence of the components of conductivity (26) in the model at hand is determined only by the functions $n_n(T)$ and $n_s(T) = n - n_n(T)$. For conventional superconductors, the experimental data are best fitted by the function $n_s(t) = n(1 - t^4)$, $t = T/T_c$, the latter leading to the known dependence $\lambda(t) = \lambda_L(1 - t^4)^{-1/2}$, $\lambda_L = (m/\mu_0 n e^2)^{1/2}$. As a result, from Eqn (26) we find $\sigma_1(T)$ and $\sigma_2(T)$, and then calculate the components $R_s(T)$ and $X_s(T)$ using Eqn (1) or (24). All the curves weakly depend on the parameter $\omega\tau < 1$ in the centimeter or longer wave bands. With a decrease of temperature $T < T_c$, when $\sigma_1 \ll \sigma_2$, according to Eqns (24) and (25) we have

$$R_s \simeq \frac{(\omega\mu_0)^{1/2}\sigma_1}{2\sigma_2^{3/2}} = \frac{1}{2}\,\omega^2\mu_0^2\sigma_1\lambda^3\,,$$
$$X_s \simeq \left(\frac{\omega\mu_0}{\sigma_2}\right)^{1/2} = \omega\mu_0\lambda\,. \quad (27)$$

The functions $X_s(T)/X_s(T_c)$ and $\sigma_2(T)/\sigma(T_c)$ quickly saturate, approaching their limiting values $(2\omega\tau)^{1/2}$ and $(\omega\tau)^{-1}$ which correspond to zero temperature, while $\sigma_1(T)$ and $R_s(T)$ tend to zero as power functions. In the opposite limiting case ($\sigma_1 \gg \sigma_2$) in close proximity to the transition temperature T_c, we have $\sigma_1 \to \sigma(T_c)$ and $\sigma_2 \to 0$, while the components of the surface impedance

$$R_s \approx \left(\frac{\omega\mu_0}{2\sigma_1}\right)^{1/2}\left(1 - \frac{\sigma_2}{2\sigma_1}\right), \qquad X_s \approx \left(\frac{\omega\mu_0}{2\sigma_1}\right)^{1/2}\left(1 + \frac{\sigma_2}{2\sigma_1}\right) \quad (28)$$

become equal at $T = T_c$ ($t = 1$). In the immediate vicinity of the transition temperature there is a very narrow peak in the curve $X_s(T)$ at $t_m = (1 - \omega\tau/\sqrt{3})^{1/4}$, which is hardly detected and whose height is $X_s(t_m) \simeq 1.14 X_s(1)$.

For further discussion it is appropriate to compare the temperature dependences of the surface impedance and complex conductivity for the two-fluid GC and microscopic BCS (weakly interacting Fermi liquid, weak coupling), and SC (strong coupling) models. The general electrodynamic relations pertaining to superconductors in the framework of the BCS and SC models are given in Ref. [69]. Using these relations, we may find simple analytic expressions for the complex conductivity in the two limiting cases of the BCS model describing London dirty and Pippard pure superconductors† at frequencies $\omega \ll \Delta/\hbar$ [70–72]:

$$\frac{\sigma_1(T)}{\sigma(T_c)} \approx \frac{\Delta(T)}{2kT}\cosh^{-2}\left(\frac{\Delta}{2kT}\right)\ln\left(\frac{\Delta}{\hbar\omega}\right),$$
$$\frac{\sigma_2(T)}{\sigma(T_c)} = \frac{\pi\Delta(T)}{\hbar\omega}\tanh\left(\frac{\Delta}{2kT}\right). \quad (29)$$

Comparing Eqns (29) and (26), it is clear that in contrast to the GC model the dependences $\sigma_s(T)$ and $Z_s(T)$ found by the BCS theory demonstrate the following peculiarities:

(1) the exponential temperature dependence $\propto \exp(-\Delta(0)/kT)$ is dominant at $T < T_c/2$;

(2) the slope of the curve $\sigma_2(T)$ as $T \to T_c$ is half that calculated from the GC model;

(3) due to the logarithmic factor in (29) the conductivity $\sigma_1(T)$ rises over the temperature interval $0.85 < T/T_c < 1$ (a coherent peak). An excess of $\sigma_1(T)$ over $\sigma(T_c)$ is in disagreement with the conventional two-fluid GC model, since the number of normal carriers n_n is required to exceed the total number of carriers n.

Nevertheless, the BCS model can be extended to the case of a two-component fluid in the London limit, if, following Ref. [72], we assume

$$n_n(T) = n - n_s(T) = nT^{-1}\frac{d\Delta}{dT}\left(\frac{d}{dT}\frac{\Delta}{T}\right)^{-1}.$$

Substituting these functions $n_s(T)$ and $n_n(T)$ into Eqn (26), we obtain the first two peculiarities typical of the BCS model. Within the two-fluid model, the temperature dependence $\sigma_1(T)/\sigma(T_c)$ passes a maximum if only the relaxation time τ depends on the energy [73].

According to the BCS theory, at an arbitrary temperature $T < T_c$ there is an energy gap Δ in the excitation spectrum, which only depends on T. For $T = 0$, quasi-particles are not produced in the BCS-superconductor and the absorption of electromagnetic waves can come into play at optical frequencies $\omega > 2\Delta(0)/\hbar$. An energy 2Δ is expended in breaking the Cooper pair and developing two excitations. As the tempera-

† Depending on the ratios between the lengths l, ξ_0, and λ at zero temperature the superconductors can be classified as pure ($l > \xi_0$), dirty ($l < \xi_0$), London ($\xi \ll \lambda$), or Pippard ($\xi \gg \lambda$). In the case of London pure superconductors $\xi = \xi_0 \ll \lambda = \lambda_L$, while in London dirty ones $\xi(l) \sim (\xi_0 l)^{1/2} \ll \lambda(l) \sim \lambda_L(\xi_0/l)^{1/2}$. In Pippard pure superconductors $\xi = \xi_0 \gg \lambda \sim \lambda_L(\xi_0/\lambda_L)^{1/3}$, and $\xi(l) \gg \lambda(l)$ in the dirty ones. The connection between the current and the field is local in London superconductors (the London limit), and essentially nonlocal in Pippard superconductors (the Pippard limit). According to this classification, HTSC single crystals are considered to be London pure superconductors rather than London dirty ones.

ture rises, the gap gets narrower and less energy $\hbar\omega$ would suffice to generate normal quasi-particles through their excitation across the gap. Just these quasi-particles are formally considered by the BCS model to be a 'normal fluid', although they are not identical to charge carriers in a normal metal due to the coherent effects of pair wave functions. The SC model was shown to be more suitable for describing the microwave response of a superconductor in terms of a two-fluid approach [74]. A feature of strongly coupled systems is the gap smearing in the spectrum of electron excitations. Strictly speaking, the gap does not occur for $T \neq 0$ at all [75, 76]. This causes the Cooper pairs to break, the peak of the density of states to be smeared, and the coherent effects to be suppressed. When the coupling constant is sufficiently large (> 2), the coherent peak of conductivity $\sigma_1(T)$ disappears and normal quasi-particles are excited through a mechanism principally different from that proposed by the BCS model [77]: they are already created without jumps across the energy gap and may find themselves in states with arbitrary energy including $\hbar\omega = 0$. Such states of quasi-particles can be thought of as gapless, while the quasi-particles arising can be treated by the two-fluid model as normal carriers. The curves $\lambda^2(0)/\lambda^2(T)$ calculated in the framework of the isotropic SC model [16, 78, 79] were found to be much like the dependence $n_s(t)/n = 1 - n_n(t)/n = 1 - t^4$ obtained by the GC model. The slope of these curves at $T = T_c$ corresponds to that measured in various YBCO single crystals and is equal to -3 [48] or -4 [25, 43, 57]. This fact as well as the evidence for the lack of a coherent peak, which is predicted by the BCS theory to occur in HTSC single crystals, point to the necessity of taking strong interactions into account near the transition temperature and to the feasibility of treating the high-frequency properties of HTSC crystals by the two-fluid approach.

4.1 The modified two-fluid model: the role of scattering effects

As was discussed in the Introduction, none of the models (GC, BCS, and SC) considered can explain the peculiarities of the surface impedance $Z_s(T)$ and conductivity $\sigma_s(T)$ typical of HTSC single crystals at low and intermediate temperatures. However, there is a simple way to treat all the observed peculiarities in the framework of the two-fluid model, modified so that it embraces the distinctive features of high-temperature superconductivity. For example, a common such feature is the high value of transition temperature T_c. At these temperatures the inelastic scattering of quasi-particles occurs in normal metals. Hence, the conventional two-fluid model can be naturally modified so as to account for the dependence $\tau(T)$.

The first attempts to ascertain the explicit form of this dependence by comparing experimental data on $\sigma_1(T)$ and $\sigma_2(T)$ with expressions (26) were made using the example of HTSC crystals, where the maximum of the real component of conductivity was observed at $T \sim T_c/2$ [21, 80, 81]. It followed from this comparison that the quantity τ should increase markedly with a reduction of temperature $T < T_c$. For some reason (insufficient quality of crystals, the use of data on $\sigma_1(T)$ and $\lambda(T)$ obtained in different experiments, etc.), however, the calculated dependences $\tau(T)$ proved to be rather exotic: $1/\tau \propto \exp(T/T_0)$, $T_0 \sim 10$ K [81] or $1/\tau \propto (AT^6 + B)$ [80]. A more detailed study was required to take into account the common and peculiar features of temperature dependences of impedance and conductivity in high-quality HTSC single crystals (see Section 3). Such an analysis was carried out by our group in Refs [25, 28, 57, 82].

The quantity $\omega\tau(T_c)$ is determined by the measured conductivity: $\omega\tau(T_c) = \sigma_1(T_c)/\sigma_2(0)$. For perfect HTSC single crystals it is equal to $\sim 10^{-3}$ in the centimeter wave band. There is no realizable mechanism to increase the relaxation time by three orders of magnitudes or more at reduced temperatures $T < T_c$. Therefore, at arbitrary temperature we have $\omega\tau \ll 1$ and expression (26) takes a very simple form within the two-liquid model:

$$\sigma_1 = \frac{e^2\tau}{m} n_n , \qquad \sigma_2 = \frac{e^2}{m\omega} n_s . \tag{30}$$

Hence, at fixed values of $n_s(t)/n$ and thus $n_n(t)/n = 1 - n_s(t)/n$, the only missing function of temperature, needed for the determination of $\sigma_s(t)$ in Eqn (30) and the impedance $Z_s(t)$ in Eqn (1), is $\tau(t)$. To be more specific, we will try firstly to describe the experimental curves $R_s(T)/R_s(T_c)$ using formula (24), substituting into it the values of $\sigma_2(T)/\sigma_2(0) = \lambda^2(0)/\lambda^2(T) = n_s(T)/n$ measured in the same experiment and data on $\sigma_1(T)/\sigma_1(T_c)$ found by (30), which, in turn, are determined by the experimental dependence $n_n(T)/n = 1 - \sigma_2(T)/\sigma_2(0)$ and an appropriately chosen dependence $\tau(T)$.

In choosing the function $\tau(T)$, we will proceed from a simple analogy between the properties of the 'normal fluid' in a superconductor and charge carriers in a normal metal. According to the Mathissen rule, at temperatures T much less than the Debye temperature Θ ($T \ll \Theta$) we have

$$\frac{1}{\tau} = \frac{1}{\tau_{imp}} + \frac{1}{\tau_{eff}} + \frac{1}{\tau_{ee}} . \tag{31}$$

The first term (scattering by impurities) does not depend on temperature, the second term corresponding to electron-phonon scattering is proportional to T^5, while the third contribution (electron–electron scattering) is proportional to T^2. Combining the first two terms we write $\tau(T)$ as

$$\frac{1}{\tau(t)} = \frac{1}{\tau(T_c)} \frac{\beta + t^5}{\beta + 1} \approx \frac{\beta + t^5}{\tau(T_c)} , \tag{32}$$

where $\beta \approx \tau(T_c)/\tau(0) \ll 1$ is a numerical parameter. Equation (32) corresponds to the low-temperature limit of the Bloch–Grüneisen formula accounting for impurity scattering. Over a wide temperature range the latter is given by

$$\frac{1}{\tau(t)} = \frac{1}{\tau(T_c)} \frac{\beta + t^5 \mathcal{J}_5(\kappa/t)/\mathcal{J}_5(\kappa)}{1 + \beta} ,$$
$$\mathcal{J}_5\left(\frac{\kappa}{t}\right) = \int_0^{\kappa/t} \frac{z^5 e^z \, dz}{(e^z - 1)^2} , \tag{33}$$

where $\kappa = \Theta/T_c$. For $\kappa \gg 1$ or, more precisely, $T < \Theta/10$ ($\kappa > 10t$), Eqn (32) follows from Eqn (33), while at $T > \Theta/5$ ($\kappa < 5t$) Eqn (33) yields the known law $1/\tau(t) \propto t$.

All the experimental curves $R_s(T)$ in high-quality YBCO single crystals can be described by the two-fluid model, for which the temperature dependence $\tau(T)$ is given by expressions (32) or (33). It is demonstrated in Fig. 15a–c, which presents the data measured in Refs [48, 25, 60] and reduced to the same frequency 10 GHz. The plot of Fig. 15b corresponds to the curve $R_s(T)$ in Fig. 6, while the data of Fig. 15c relates

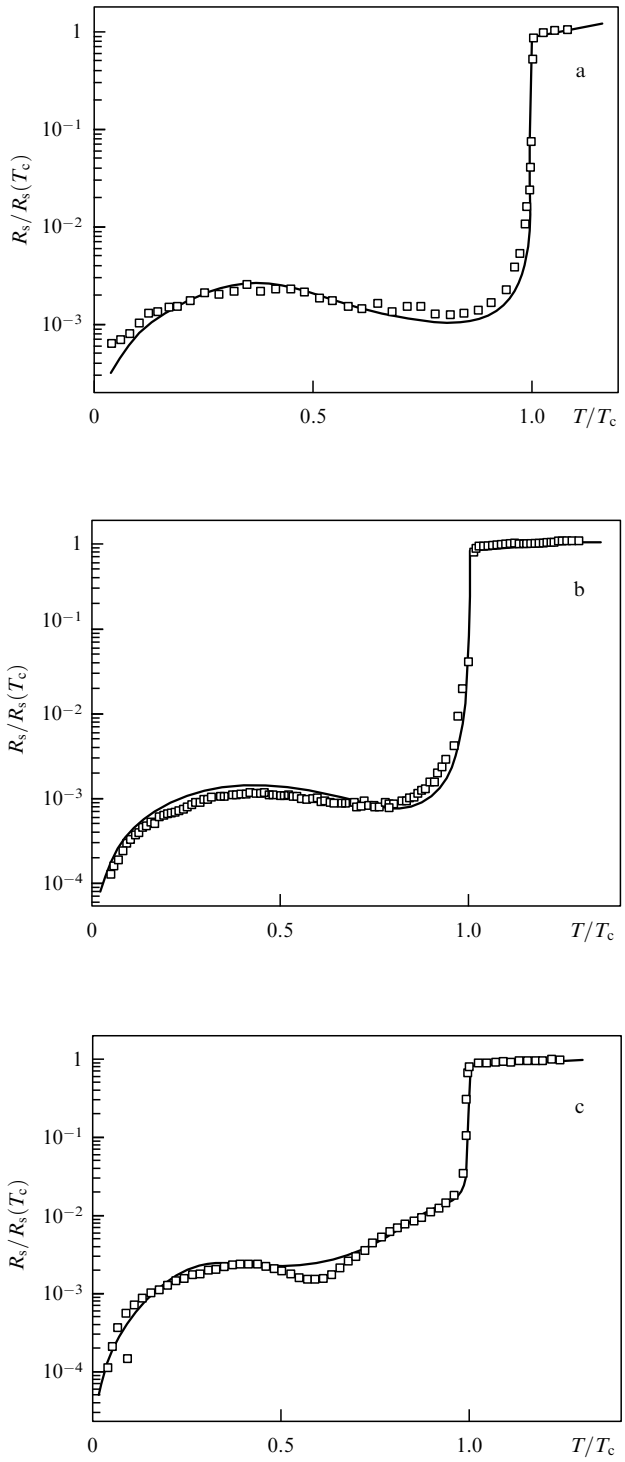

Figure 15. Comparison of the calculated (solid lines) and measured (squares) dependences of the surface resistance $R_s(T)/R_s(T_c)$ in YBCO single crystals. The experimental data are taken from Refs [48] (a, 4.13 GHz), [25] (b, 9.42 GHz), and [60] (c, 10 GHz) and converted ($\propto \omega^{3/2}$) to the same frequency 10 GHz.

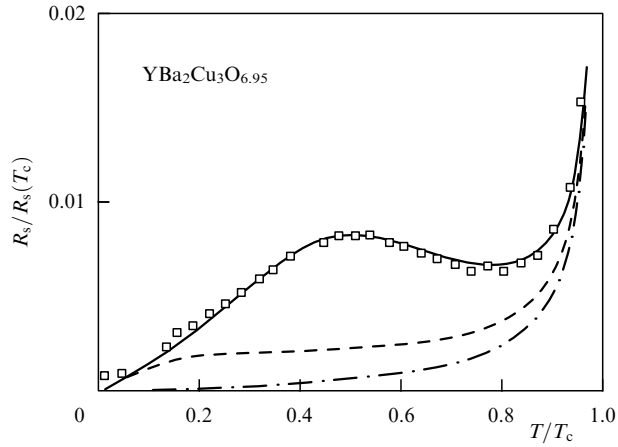

Figure 16. Experimental (squares) and calculated (lines) data on the surface resistance of a YBCO single crystal; the measurements were taken on a frequency of 34.8 GHz [48]. The lines were obtained using (24). The dashed line corresponds to the replacement of t^5 by t^2 in the numerator of (32), and the dot-and-dash line to the temperature-independent relaxation time.

to curve *1* in the inset to Fig. 12. At this frequency the values of $\omega\tau(T_c) = [\rho(T_c)\sigma_2(0)]^{-1}$ were about 4×10^{-3}, i.e. $1/\tau(T_c) \approx 2 \times 10^{13}$ s^{-1} in the experiments [48, 25, 60]. The solid lines in Fig. 15 present calculations of $R_s(T)/R_s(T_c)$ using formulae (24) and (30), where we used the values of $\sigma_2(T)/\sigma_2(0)$ measured in the same experiments [48, 25, 60] and plotted below in Fig.18a – c. The curve in Fig. 15a was constructed using the single fitting parameter $\beta = 0.01$ in Eqn (32), while the curve of Fig. 15b corresponded to $\beta = 0.2$ in Eqn (32) and the curve in Fig. 15c was obtained at $\beta = 0.02$ and $\kappa = 4$ in Eqn (33). The calculated curves virtually coincide with the experimental findings over the whole temperature range and indicate the common and peculiar features of the surface resistance $R_s(T)$ in YBCO single crystals fabricated in different ways. Namely, one can see a wide maximum at intermediate temperatures, caused by a fast increase in the relaxation time $\tau(T) \propto T^{-5}$ at reduced temperatures, and the growth of $R_s(T)$ observed in Ref. [60] over the temperature interval $T_c/2 < T < T_c$ (Fig. 15c). The latter phenomenon is associated with the change from the regime of temperature variation $\sim T^{-5}$ to that of $\sim T^{-1}$ in Eqn (33) for $\tau(T)$, which occurs in this crystal (see Fig. 15c) at lower (as compared to Fig.15a, b) temperatures. Thus, one can come to recognize that the electron – phonon scattering of normal quasi-particles makes the main contribution to the formation of signal $R_s(T)$ in YBCO single crystals.

Figure 16 plots on a linear scale the experimental data on $R_s(T)$ measured in Ref. [48] for the same sample as in Fig. 15a but at a higher frequency, for which we used the value of $\omega\tau(T_c) \approx 1.5 \times 10^{-2}$ (solid line). The dashed line in the figure corresponds to the temperature dependence given by formula (32), for which $1/\tau(t)$ is proportional to t^2 instead of t^5, while the dot-and-dash line plots the same dependence when the relaxation time τ does not depend on temperature at all. It should be reiterated that a wide peak of $R_s(T)$ around $T \sim 0.4T_c$, which is typical of YBCO samples, arises only when we use $1/\tau(t) \propto t^5$. Besides, only such a temperature dependence of the relaxation time results in a pronounced elevation of $R_s(T)$ over a wide temperature range, the latter being a common feature of HTSC compounds.

Accounting for the third term in Eqn (31), i.e. the addition of a term quadratic in temperature to the numerator of Eqn (33), flattens the peak. This is significant in comparing the model dependences with the results measured in HTSC single crystals with tetragonal structure, where a wide peak in $R_s(T)$ (typical of YBCO crystals) is not observed. Figure 17 compares experimental (symbols) and calculated (lines) data on the surface resistance in BSCCO single crystals, measured

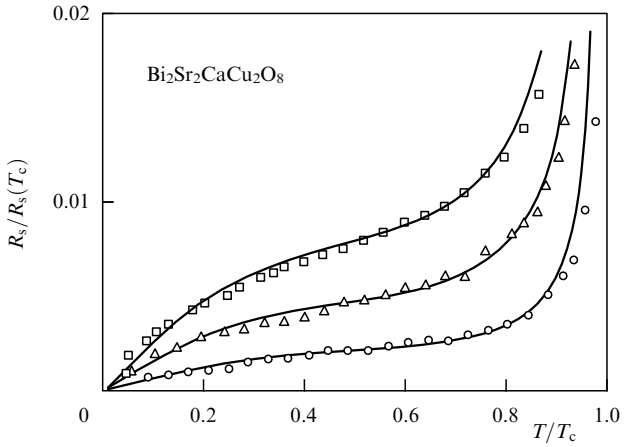

Figure 17. Experimental (symbols) and calculated (lines) data on the surface resistance of a BSCCO single crystal; the measurements were made at various frequencies: (○) 14.4 GHz, (△) 24.6 GHz, (□) 34.7 GHz [56]. The solid lines present the curves $R_s(T)/R_s(T_c)$ calculated at the frequencies given.

at various frequencies [56]: 14.4 GHz ($\omega\tau(T_c) = 0.8 \times 10^{-2}$), 24.6 GHz, and 34.7 GHz. The theoretical curves are constructed starting from formulae (24) and (30) at the relevant frequencies and using experimental data on $\sigma_2(T)/\sigma_2(0) = n_s(T)/n$, taken from Ref. [56], and the dependence

$$\frac{1}{\tau(t)} = \frac{\beta + \gamma t^2 + t^5}{\tau(T_c)(\beta + \gamma + 1)}\,, \tag{34}$$

where $\beta = 0.1$ and $\gamma = 0.9$.

Figures 15–17 presenting measurements of the surface impedance of various crystals at different frequencies demonstrate a good agreement between the experimental data and the dependences $R_s(T)$ calculated in the framework of the two-fluid model.

4.2 Temperature dependence of the density of superconducting electrons

Let us try now to describe the experimental curves $\sigma_2(T)/\sigma_2(0)$ in themselves. Figure 18a plots the dependence $\lambda^2(0)/\lambda^2(t) = n_s(t)/n$ for the *ab*-plane of a YBCO single crystal [48]. Similar dependences with slightly changed slopes at low temperatures and near the transition temperature T_c were obtained in other experiments on YBCO samples [43, 44], as well as BSCCO [54, 56] and TBCO [58] crystals with a tetragonal structure. The dependences are linear at low temperatures and well described by the relation

$$\frac{n_s}{n} = (1 - t)^{\alpha}\,, \tag{35}$$

where α is a numerical parameter. For $t \ll 1$, we have $n_s(t)/n = \sigma_2(t)/\sigma_2(0) \simeq (1 - \alpha t)$. For the experiments considered the parameter α varies from 0.5 to 0.7. The solid line in Fig. 18a depicts dependence (35) at $\alpha = 0.5$. Near the transition temperature T_c we find $\lambda(t) \propto n_s(t)^{-1/2} \propto (1 - t)^{-\alpha/2}$, which also agrees fairly well with the experimental data. Perhaps, the only drawback of formula (35) for describing typical data on $\sigma_2(T)$ in Fig. 18a is the infinite derivative $d\sigma_2(t)/dt \propto (1 - t)^{\alpha - 1}$ for $t = 1$ and $\alpha < 1$.

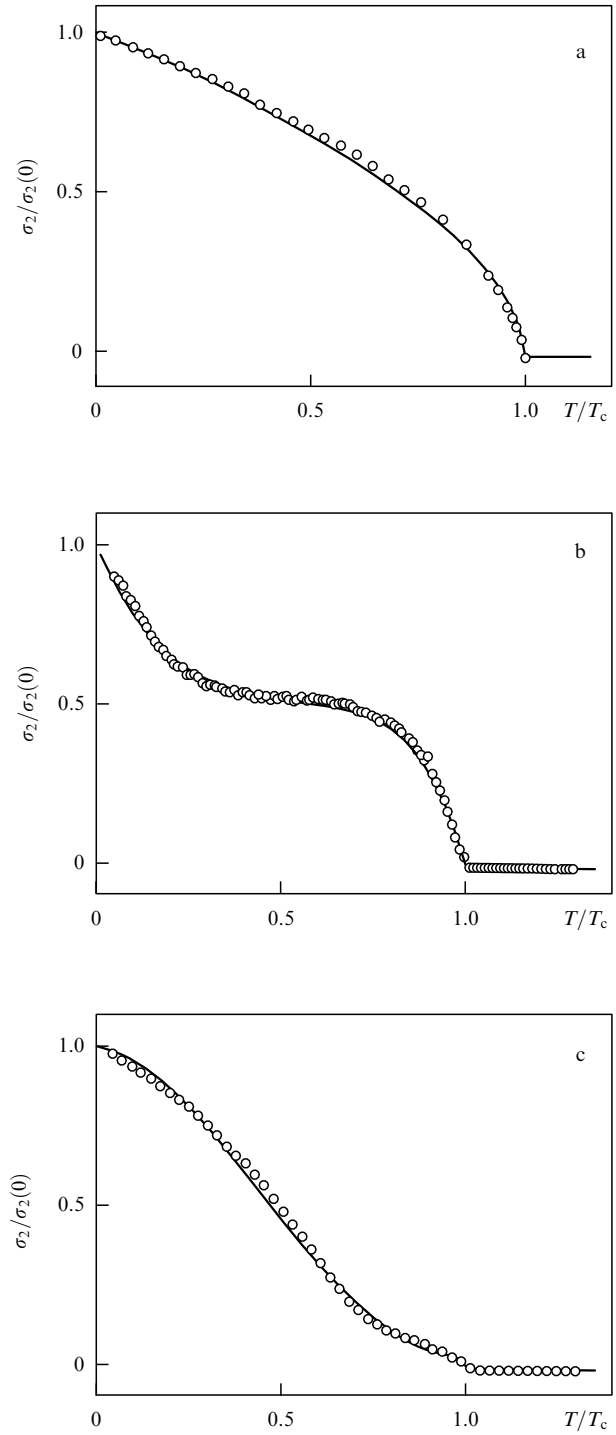

Figure 18. Comparison of calculated (lines) and experimental (symbols) dependences $\sigma_2(T)/\sigma_2(0) = \lambda^2(0)/\lambda^2(T)$ in YBCO single crystals. The experimental data are taken from Refs [48] (a), [25] (b), and [60] (c).

However, a simple relation for $n_s(t)$ in Eqn (35) does not describe the peculiarities of dependences $\lambda^2(0)/\lambda^2(T)$, which have recently been observed in YBCO single crystals at intermediate temperatures [25, 57, 60, 61]. Besides, if we treat the dependences using (35), then the slope of the curves at $T \ll T_c$ corresponds to $\alpha > 1$, resulting in a zero slope for the curves $\sigma_2(T)/\sigma_2(0)$ at the point $T = T_c$. Therefore we should introduce one more term to the right-hand side of Eqn (35) without violating the condition $n_s + n_n = n$ met in the

two-fluid model:

$$\frac{n_s}{n} = (1-t)^{\alpha}(1-\delta) + \delta(1-t^{4/\delta}) , \tag{36}$$

where $0 < \delta < 1$ is a weight factor. For $\delta \ll 1$ ($\delta \to 0$) and $\alpha > 1$ the first term in the right-hand side of (36) is dominant everywhere over the temperature interval, while the second term only ensures a finite slope of the dependence $\sigma_2(T)/\sigma_2(0)$ at $T = T_c$, which is equal to -4 in accordance with the GC model. As the parameter δ rises, the influence of the second term in Eqn (36) strengthens. The experimental dependence $\sigma_2(T)/\sigma_2(0)$ in Fig. 18b, derived using formula (25) from the data on $R_s(T)$ and $X_s(T)$ presented in Fig. 6, is well fitted by formula (36) at $\delta = 0.5$ and $\alpha = 5.5$. The fitted dependence reveals features typical of the measurement results: at low temperatures the dependence is linear and its second derivative is positive ($\alpha > 1$); at intermediate temperatures there is a plateau resulting from equal ($\delta = 0.5$) contributions of both the terms in (36), and finally the slope of the fitted dependence near T_c is consistent with the experiment. All the curves $\sigma_2(T)$ we measured in the *ab* plane of YBCO crystals (grown by the same method at ISSP) were described by formula (36) where the parameter $\alpha \approx 5.5$ was practically unchanged, while the parameter δ varied within the interval $0.1 < \delta \leqslant 0.5$.

The third curve in Fig. 18c, taken from Ref. [60] and corresponding to $\lambda(T)$ (Fig. 12, curve *1*), differs from the typical curves presented in Fig. 18a or Fig. 12 (*2*, *3*). The difference implies that the linear section of $\sigma_2(T)$ lies in a shorter temperature interval $0 < T \ll T_c$ and is steeply transformed to being quadratic at increased temperatures. This transformation can be described by introducing an additional multiplier $(1 + \eta t)$ into the first term of (36) [25]. Then for $\alpha = 2.2$, $\eta = 2$, and $\delta = 0.04$ we arrive at the solid line in Fig. 18c.

Thus, treating the data in the framework of the two-fluid model based on Eqns (30)–(36), we can describe the common features of the dependences $Z_s(T)$ and $\sigma_s(T)$ for high-quality HTSC single crystals. At low temperatures, $t \ll 1$, all the dependences have linear sections: $\sigma_1 \propto \alpha t/\beta$, since $n_n/n \approx \alpha t$ and $\tau \approx \tau(0) \approx \tau(T_c)/\beta$; $\Delta\sigma_2 \propto -\alpha t$; $R_s \propto \alpha t/\beta$, according to (27), and $\Delta X_s \propto \Delta\lambda \propto \alpha t/2$. As the temperature rises the function $\sigma_1(t)$ passes a maximum at $t < 0.5$. The maximum results from the combined action of two opposite effects such as the decreased number of normal carriers at reduced temperatures $t < 1$ and the increase of relaxation time, which terminates at $t \sim \beta^{1/5}$. The two-fluid model considered is also suitable for revealing peculiarities of temperature dependences of the surface resistance and complex conductivity in YBCO single crystals grown by various methods.

5. On the way to the microscopic theory

There are a huge number of papers and reviews [74, 83–89] devoted to theoretical investigations of mechanisms of superconductivity in HTSC compounds. This literature usually deals with some particular conceptually possible mechanism of electron pairing in terms of which some available experimental data are described†. Now there is neither a conventional microscopic theory of the high-temperature superconductivity as a whole, nor a microscopic model of the high-frequency response of an HTSC in particular. The trouble is dramatized by experimenters who are revealing new properties of HTSCs as the quality of samples and measuring techniques are being improved. The peculiarities of the temperature dependence of the surface impedance of high-quality YBCO single crystals is an example of such an event in the microwave measurements. While in 1994 it seemed that all the measurement data on $Z_s(T)$ and $\sigma_s(T)$ known for YBCO crystals [48] could be explained by the simple *d*-wave model [90–92], the studies of the last three years have spoiled this impression.

Leaving aside possible mechanisms of superconducting pairing, we will analyze briefly the available microscopic theories of the high-frequency response in HTSCs. Since the phenomenological model formulated in the previous section is in a good agreement with the experimental data on $Z_s(T)$ of HTSC single crystals, it is appropriate to compare the simple model with the results of the microscopic consideration. Perhaps, we will succeed in developing a general microscopic approach to describing the microwave properties of HTSCs.

5.1 The isotropic SC model and the relaxation time in the superconducting state

The Eliashberg equations accounting for retardation and damping of quasi-particles can be used to describe superconductors with an arbitrarily strong interaction between Fermi particles. We will consider electron-phonon interactions in an isotropic single-band superconductor with a singlet *s*-pairing and the Debye phonon spectrum, and ignore phonon corrections to the electromagnetic vertex (referred to as the vertex correction) when solving the Eliashberg equations. Then the function $\Gamma(T) = 1/2\tau(T)$ corresponding to the damping coefficient of quasi-particles is proportional to T^3 at temperatures $T < T_c$ [14, 74]. If these corrections are taken into account, then according to Ref. [93], $\Gamma(T) \propto T^5$, which is in agreement with Eqn (32). Using this conclusion, the authors of Ref. [13] showed that the temperature dependences $R_s(T)$ and $\sigma_1(T)$ have wide peaks typical of YBCO samples within the framework of the conventional isotropic SC model, although there is a quantitative disagreement between the theory and experiment. To our knowledge paper [93] is still the only work where the vertex corrections are taken into account. It would be interesting to know whether the conclusion of Ref. [93] is correct for other microscopic models which are more suitable for describing HTSCs.

5.2 Model of an almost antiferromagnetic Fermi liquid with *d*-pairing

In this model, the low-frequency excitations are not phonons but weakly damping spin waves, while the pairing is provided by spin fluctuations [94–96]. The paramagnon mechanism of pairing leads to the *d*-symmetry of the order parameter when there are gapless lines on the Fermi surface. The latter means that the normal excitations in the superconductor exist even at zero temperature $T = 0$, resulting in particular in a finite conductivity [97]

$$\sigma_{\min} = \frac{ne^2}{m\pi\Delta_0} = \frac{2\Gamma(T_c)\sigma(T_c)}{\pi\Delta_0} , \tag{37}$$

where $2\Gamma(T_c) = 1/\tau(T_c)$, and Δ_0 is the gap maximum on the Fermi surface, which is equal to $\Delta_0 = 2.14T_c$ without regard

† An exception is the review [87] comparing various theoretical approaches.

for strong coupling effects (from here on we use units in which $\hbar = k = 1$). Remembering the value $2\Gamma(T_c) = 2 \times 10^{13}\ \mathrm{s}^{-1} \simeq 0.8T_c$, for YBCO single crystals [25, 48, 60] we estimate $\sigma_{\min} \simeq 0.1\sigma(T_c)$ from (37). Substituting the latter into formula (27) we arrive at the minimal surface resistance $R_{s\,\min}$ of a superconductor with d-pairing. On a frequency of 10 GHz, the minimal resistance is $R_{s\,\min} \sim 1\ \mu\Omega$ in YBCO samples, i.e. an order of magnitude lower than the experimental values obtained so far.

Such unusual (from the traditional standpoint) manifestations of d-symmetry have stimulated theoretical treatment of various properties of HTSC with the model of an almost antiferromagnetic Fermi liquid.

The dependences $\sigma_s(T)$ and $R_s(T)$ were calculated in Refs [90–92] and compared with the experimental data of Ref. [48]. Let us discuss the problem in greater detail.

Firstly, we consider the case of the relatively low temperatures $T < 0.4T_c$, when the damping of quasi-particles is due to scattering by impurities. According to Refs [90–92], in this range we have:

(1) integral expressions describing the microwave response of the superconductor admitting a conductivity representation as (26) or (30), where $\tau(T) \approx \tau(0) \equiv 1/2\Gamma$, and Γ is the frequency of elastic relaxation; the latter is significantly less than $\Gamma(T_c)$, for example, in the experiment [48] $\Gamma/\Gamma(T_c) \simeq \tau(T_c)/\tau(5\,\mathrm{K}) \simeq \beta \approx 0.01$;

(2) the scattering is restricted by the weak (Born) and strong (unitary) limits with the phase shifts equal to $\delta = 0$ and $\delta = \pi/2$, respectively. In the Born approximation, the transition temperature T_c should be reduced significantly, but this is not examined experimentally;

(3) there is a crossover temperature T^* separating the 'gapless' ($T < T^* \ll T_c$) and 'pure' ($T^* < T \ll T_c$) regimes. Under the conditions of the unitary limit close to the experimental ones, the crossover temperature is $T^* \approx 0.8(\Gamma\Delta_0)^{1/2} \approx 0.1T_c \simeq 9$ K in the case of perfect YBCO crystals with optimal doping. The addition of impurities (for example, Zn used in Ref. [48]) increases the frequency Γ of elastic relaxation and the crossover temperature T^*.

In the 'pure' regime the penetration depth depends linearly on the temperature $t = T/T_c$:

$$\frac{\lambda(t)}{\lambda(0)} = 1 + c_1 t\,, \qquad c_1 = \frac{T_c \ln 2}{\Delta_0}\,. \tag{38}$$

The dependence agrees with Eqn (35), which yields

$$\frac{\lambda(t)}{\lambda(0)} = 1 + \frac{\alpha t}{2}\,, \qquad t \ll 1\,. \tag{39}$$

Equating $\alpha = 0.5$ (Fig. 18a) and $2c_1$ determined by expression (38), we estimate the experimental quantity $\Delta_0 \simeq 2.7T_c$ [48]. At frequencies of 4 GHz ($\omega/T_c \simeq 0.002$) and 35 GHz ($\omega/T_c \simeq 0{,}019$), the value of ω/Γ is approximately equal to $0.2T_c$ and $1.9T_c$, respectively [48], corresponding to the intermediate range between the hydrodynamic ($\omega/\Gamma \ll 1$) and collisionless ($\omega/\Gamma \gg 1$) limits. According to computations [91, 92], the conductivity $\sigma_1(T)$ linearly depends on T in this range (essentially suitable for the measurements at 35 GHz in Ref. [48]). As is seen from Fig. 9 of Ref. [92], the slope of the curve $\sigma_1(T)/\sigma(T_c)$ at $T \ll T_c$ is close to the value of α/β calculated using the phenomenological model.

As the concentration of impurities rises at low temperatures, the pure regime gives way to a gapless one, while the intermediate regime changes to the hydrodynamic one, resulting in the typical dependences $\Delta\lambda(T) \propto T^2$ and $\sigma_1(T) \propto T^2$. Both the dependences agree with the experimental data [48], where Cu atoms in YBCO samples are replaced by Zn atoms.

Inelastic scattering is significant at temperatures $T > 0.4T_c$. The temperature dependence of the damping coefficient for quasi-particles scattered by spin fluctuations was calculated in Ref. [98] without regard for vertex corrections and appeared proportional to T^3, $1/\tau(T) \propto T^3$. Taking this conclusion into account, the authors of Refs [91, 92] calculated the surface resistance and conductivity at intermediate temperatures and in the region near the transition temperature T_c and found the peaks in $\sigma_1(T)$ and $R_s(T)$. Unfortunately, they used an overly decreased value of $\Gamma/T_c = 0.0008$, which does not enable us to compare the theoretical and experimental data in detail. We note only that the calculated peak of $R_s(T)$ is shifted to lower temperatures with respect to the experimental one [48]; the latter is probably caused by the temperature dependence $1/\tau$ being insufficiently strong (see Fig.16).

Thus, the d-wave model of microwave response [90–92] qualitatively describes the low-temperature dependences of the surface impedance and conductivity measured in YBCO crystals [48] and formally agrees with the above-considered phenomenological two-fluid model at $T \ll T_c$. The advantage of papers [90–92] is that the model manifests nontrivial consequences of d-symmetry of the order parameter, using few fitting parameters to describe the microwave measurements of the first high-quality YBCO single crystals. The $\sigma_2(T)$ curves measured in the HTSC crystals with a tetragonal structure (see Fig. 18a) could also be explained by the model. But it fails to account for the linear dependence of $R_s(T)$ in the temperature range up to $T_c/2$ at frequencies ~ 10 GHz. Neither can it explain the possibility of an essentially different slope of $\sigma_2(T)$ at $T \ll T_c$ (corresponding to $\alpha > 1$ in Eqn (36), which according to (38) would have yielded $\Delta_0 < T_c$) in the experiments [25, 57, 60, 61] with YBCO single crystals. The model can hardly be used to describe the peculiarities at intermediate temperatures and the increased slope of $R_s(T)$ and $\sigma_2(T)$ in the limit $T \to T_c$.

The above approach was further developed in Ref. [62] where the calculated dependences $Z_s(T)$ were compared with the data measured on a frequency of 87 GHz in two different YBCO films. The authors of Ref. [62] theoretically studied the evolution of the dependences $\sigma_s(T)$ and $R_s(T)$ in passing from the unitary limit to the Born one and showed that the value of minimal conductivity described by (37) was not universal, and the experimental results were best fitted by the intermediate phase shift $\delta \approx 0.4\pi$. The optimal coincidence requires six (or even nine) fitting parameters. Three parameters are necessary to describe phenomenologically the temperature dependence of the inelastic relaxation time

$$\frac{\tau(1)}{\tau(t)} = at^3 + (1-a)\exp\{b_1(t-1)[1 + b_2(t-1)^2]\}, \quad t = \frac{T}{T_c}.$$

In the case of the higher-quality film (b) used in Ref. [62], the parameter $a = 0$, and the remaining terms are well approximated by $1/\tau(T) \propto T^5$. The calculation method developed in Ref. [62] and its modification to the case of strong coupling [99] would be useful in considering experimental data on HTSC single crystals in the centimeter wave band.

5.3 The two-band model and mixed symmetry of the order parameter

The peculiarities of $Z_s(T)$ and $\sigma_s(T)$ curves recently revealed in YBCO single crystals [25, 57, 60, 61] can be explained by a two-band model or by the mixed symmetry of the order parameter. The shape of the experimental dependences (Fig. 18b and c) alone and function (36) describing them and containing two terms give grounds to this suggestion. Besides, the order parameter has a mixed $(d+s)$-symmetry coinciding with the symmetry of the orthorhombic lattice and this type of symmetry is more natural for YBCO crystals than the pure d-symmetry typical of tetragonal structures.

HTSC crystals were first treated by the two-band model in a series of papers [100]. The model is an extension of the SC theory to the case of layered HTSC, particularly, to YBCO systems where two subsystems occur: a band of CuO_2 planes (S-band) and a band of CuO chains (N-band). The temperature and concentration dependences of the density of states in this system were considered in Ref. [101].

In calculating the microwave response [18, 102, 103], a strong electron-phonon interaction in the S-band and weak superconductivity in the N-band, caused by proximity effects, were assumed. A set of coupled Eliashberg equations was solved to find an s-type order parameter and the renormalization functions in each of the bands [18, 102]. The parameters of the equations were the coupling constants λ_{ij} and the coefficients γ_{ij} and γ_{ij}^M for the transition from ith band into the jth band due to the relevant scattering by ordinary and magnetic impurities.

In Refs [18, 103], the number and values of the parameters were fitted from the experimental data known for YBCO single crystals. In the case of the S-band $\lambda_{11} = 3$, while $\lambda_{22} = 0$ in the N-band, a nonzero gap for CuO chains was induced by the interband interaction for which $\lambda_{12} = \lambda_{21} = 0.2$. The chosen set of coupling constants led to $T_c = 92$ K. The interband scattering effects were supposed to be negligible, i.e. $\gamma_{12}, \gamma_{21} \ll T_c$. The intraband scattering in each band was taken into account through the coefficients γ_{11} and γ_{22}. The scattering by magnetic impurities ($\gamma_{22}^M \equiv \gamma^M$) occurred only in the N-band ($\gamma_{11}^M = 0$) where oxygen atoms are most flexible, and leaving CuO chains they produced magnetic moments on uncompensated copper ions Cu^{2+}. The parameter γ^M is proportional to the concentration of magnetic impurities, which grow in number as the oxygen concentration in the sample decreases. The coefficients of elastic relaxation in the bands were assumed to be the same $\gamma_{11} = \gamma_{22} \equiv \gamma^{\text{imp}}$ and estimated from the absolute value and anisotropy of resistivity of YBCO crystals in the normal state. The values of γ^{imp} in the interval $2 \leqslant \gamma^{\text{imp}}/T_c \leqslant 4$ correspond to the measured values $50 \leqslant \rho(100\text{ K}) \leqslant 100\ \mu\Omega\,\text{cm}$ and anisotropy ρ equal to 2 in the ab-plane. Note that γ^{imp} differs from $\Gamma = 1/2\tau(0)$ used in the models considering a single band. The inelastic scattering coefficients reasonably appeared proportional to T^3 for the Debye phonon spectrum [18, 103] and did not include vertex corrections to the conductivity. Thus, the large number of parameters initially contained in the Eliashberg equations describing the two-band model reduce in reality to four parameters λ_{11}, λ_{12}, γ^{imp}, and γ^M, two of which ($\lambda_{11} = 3$ and $\lambda_{12} = 0.2$) are fixed, and two others (γ^{imp} and γ^M) are varied.

Figure 19 plots the calculated and experimental temperature dependences $\sigma_2(T)/\sigma_2(0)$. The experimental data are taken from Refs [43, 48] and given in Fig.18a. For all the curves (*1–4*) the parameter $\gamma^M = 0.2T_c = \text{const}$, and they differ only in the increasing parameter γ^{imp}: $2T_c$ (*1*), $4T_c$ (*2*), $8T_c$ (*3*), and $20T_c$ (*4*). The inset to Fig. 19 depicts the influence of the magnetic scattering (oxygen content of YBCO). In the case of complete oxidation of the sample, magnetic scatterers are absent in the chains (N-band) and $\gamma^M = 0$. The calculations using the two-band model (curve *1* in the inset) and the experimental data (■) obtained for YBCO films [42] result in an exponential dependence of $\Delta\lambda_{ab}(T)$ for $T \ll T_c$†, caused by a narrow gap induced in the N-band. The appearance of a few magnetic scatterers ($\gamma^M = 0.1T_c$, curve *2*) enhances the slope of the curve $\Delta\lambda_{ab}(T)$, the dependence remaining exponential. However, a further increase in the parameter γ^M (removal of oxygen) changes the exponential dependence $\Delta\lambda_{ab}(T)$ into a linear one, since the superconducting state in the chains becomes gapless at $T > 0.05T_c \approx 5$ K. A similar linear dependence $\Delta\lambda_{ab}(T)$ ($\gamma^M = 0{,}3T_c$, $\gamma^{\text{imp}} = 4T_c$) is depicted in Fig. 2, where it is compared with the data measured in the YBCO film at 87 GHz [17]. At sufficiently high values of γ^{imp}, the N-band does not affect the penetration depth, and the dependence $\Delta\lambda(T)$ becomes similar to that predicted by the isotropic SC model: $\Delta\lambda(T) \propto T^n$, where the power index exceeds 2 [14, 93]. A transformation from the linear dependence $\Delta\lambda(T)$ to a power one ($n = 4$), as the concentration of impurities increased, was recently observed in YBCO crystals [106], where the Y atoms were replaced by Pr ions.

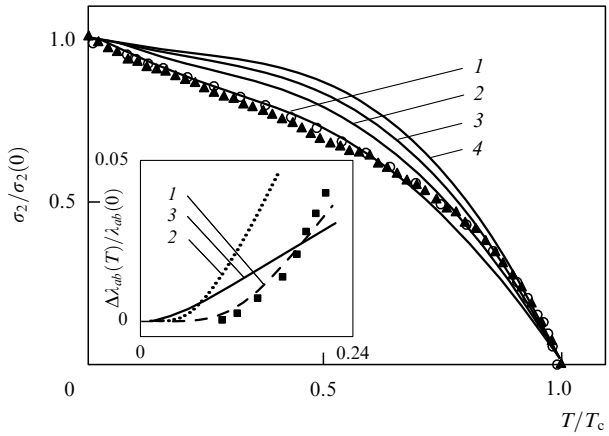

Figure 19. Comparison of calculated (lines) and experimental (symbols) temperature dependences $\sigma_2(T)/\sigma_2(0)$. The symbols (▲) and (○) correspond to the experimental data taken from Refs [43] and [48], respectively; the calculated curves correspond to $\gamma^M = 0.2T_c$: (*1*) $\gamma^{\text{imp}} = 2T_c$, (*2*) $\gamma^{\text{imp}} = 4T_c$, (*3*) $\gamma^{\text{imp}} = 8T_c$, and (*4*) $\gamma^{\text{imp}} = 20T_c$. The inset ($\gamma^{\text{imp}} = 2T_c$) depicts a crossover from the exponential (curves *1*, $\gamma^M = 0$ and *2*, $\gamma^M = 0.1T_c$) to the linear (curve *3*, $\gamma^M = 0.4T_c$) temperature dependences of $\Delta\lambda_{ab}(T)$ as the concentration of magnetic impurities rises. The squares show the data measured in Ref. [42].

The complex conductivity $\sigma_s = \sigma_1 - i\sigma_2$ in a two-band superconductor includes the conductivity of the S-band ($\sigma_s^S = \sigma_1^S - i\sigma_2^S$) and N-band ($\sigma_s^N = \sigma_1^N - i\sigma_2^N$):

$$\sigma_s = \sigma_s^S + \zeta\sigma_s^N\,, \qquad \zeta = \frac{v^S m^N}{v^N m^S}\,, \tag{40}$$

† So far the exponential dependence $\Delta\lambda(T)$ has been observed only in a single study on high-quality YBCO films [42, 104], which quickly degraded with time [105]. Perfect HTSC single crystals do not exhibit such exponential behaviour. Note that the activation dependences $\sigma_s(T)$ and $R_s(T)$ are incompatible with the d-wave symmetry of the order parameter.

where $v^{S,N}$ and $m^{S,N}$ are the densities of states and masses of carriers in the relevant bands. The dependences $\sigma_1(T)$ and $R_s(T)$ calculated in Ref. [103] agree with the data measured in YBCO samples [17], although they are not detailed at low temperatures and in the region near the transition temperature T_c.

Despite the obvious advantages of the two-band model, it can hardly be used to describe microwave measurements in HTSC single crystals with tetragonal structure which do not contain CuO chains and, hence, such evident magnetic scatterers as in YBCO samples. Meanwhile, the magnetic scatterers play a key role: they make the gap of the N-band equal to zero and give rise to a linear temperature dependence $\Delta\lambda_{ab}(T)$ at $T \ll T_c$. The d-symmetry of the order parameter in a superconductor eliminates the problem‡. In addition, the peculiarities of the experimental data on $Z_s(T)$ and $\sigma_s(T)$ in YBCO single crystals at intermediate temperatures cannot be explained by s-pairing in both the bands. Therefore it seems natural to introduce a d-symmetric order parameter for one of the bands§. Recently such an attempt has been made [112] and the calculated dependence $\sigma_2(T)/\sigma_2(0)$ is plotted in Fig. 20. Within the model the S-band has the d-symmetry of the gap, while the N-band has the s-symmetry; the model parameters are $\lambda_{11} = 3$ and $\lambda_{22} = 0.5$ and only the interband scattering is taken into account in formula (40) with $\zeta = 0.5$ and $\gamma_{12} = \gamma_{21} \equiv \gamma$. The solid line in Fig. 20 demonstrates the peculiarity at $T \approx 0.6T_c$ disappearing when the disorder is enhanced. A similar approach was used in Ref. [61] to explain the experimental data, particularly, to describe phenomenologically the curve in Fig. 18c. It should be noted that the consequences of the mixed $(d+s)$-symmetry of the order parameter and properties of HTSCs related to microwaves are topical today (see, for example, Refs [113–116]), and interesting findings are to be expected.

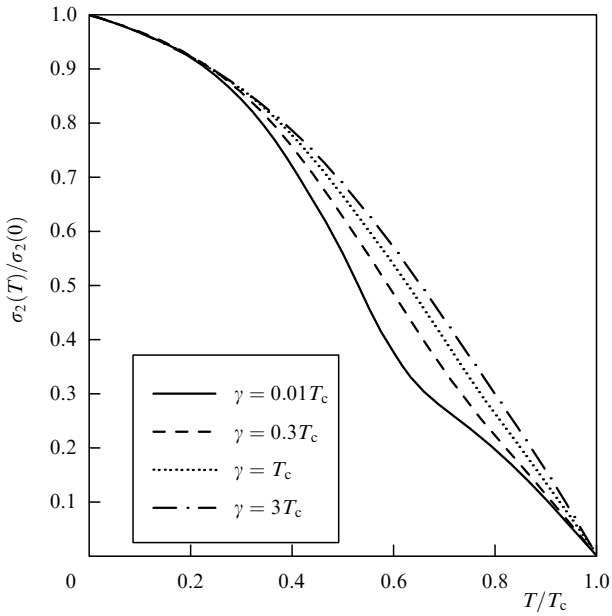

Figure 20. Changes in the curves $\sigma_2(T)/\sigma_2(0)$, caused by variations in the coefficient of interband scattering γ. The data are calculated using the two-band model dealing with the d-symmetry of the order parameter for the S-band and s-symmetry for the N-band [112].

6. Conclusions

We have tried to classify and generalize the data of measurements on the surface impedance $Z_s(T) = R_s(T) + iX_s(T)$ of high-quality YBCO, BKBO, TBCCO, TBCO, and BSCCO single crystals in the temperature range $4.2 \leqslant T \leqslant 150$ K. The common features for all the crystals are the linear dependences of the surface resistance $\Delta R_s(T) \propto T$ and reactance $\Delta X_s(T) \propto \Delta\lambda_{ab}(T) \propto T$ at temperatures far from the transition temperature ($T \ll T_c$), the sharp increase as $T \to T_c$, and the root dependence $R_s(T) = X_s(T) = \sqrt{\omega\mu_0\rho(T)/2}$ corresponding to a linear variation of $\Delta\rho_{ab}(T) \propto T$ in the normal state. We detected that the dependences $Z_s(T)$ in BSCCO, TBCCO, and TBCO single crystals with a tetragonal structure and in BKBO samples with a cubic structure differ from those in YBCO crystals with an orthorhombic structure. In the tetragonal structures the linear section of $\Delta R_s(T) \propto T$ may extend up to $T_c/2$ at frequencies ~ 10 GHz, while the linear behaviour at $T < T_c/3$ changes to a wide peak of $R_s(T)$ in YBCO crystals. In addition, YBCO single crystals exhibit peculiarities of the $\lambda_{ab}(T)$ dependences at intermediate temperatures.

We have described all the above effects in $Z_s(T)$ in the framework of the two-fluid model taking into account the scattering of quasi-particles and the changed density of superconducting carriers at low temperatures and in the region near the transition temperature. The suggestions of the model may be important in developing a microscopic theory of high-frequency response in HTSCs.

We have considered in detail the microwave properties of high-quality HTSC single crystals with optimal doping only, since there is a large body of experimental data on such crystals. But three important problems appeared beyond the scope of our consideration and we should outline them.

Firstly, changes in the temperature dependence $Z_s(T)$, caused by deviations from the optimal doping, have not been adequately investigated. There are no experimental data on the microwave properties of a crystal where the concentration of carriers is varied but controlled. At the same time, the problem of doping effects tightly relates to the available symmetry of the order parameter [87, 117], changes in the pseudogap [88, 89, 118], and the superconductor–insulator transition [119], which are important in explaining the microscopic properties of HTSCs.

Secondly, the origin of the residual surface resistance observed in HTSC single crystals is still unclear. The influence of surface cleaning on the dependence $Z_s(T)$ has not been studied, although there are a number of phenomenological [120–126] and microscopic [127–132] models

‡ The third law of thermodynamics forbids the linear dependence $\Delta\lambda(T) \propto T$ at ultralow temperatures $T \to 0$ [107]. This means that there is always a crossover temperature $T^* \ll T_c$, below which the dependence $\Delta\lambda(T)$ is not linear for a superconductor with a d-gap. At present two such mechanisms resulting in a crossover temperature are known, namely, scattering by impurities [90] and nonlocal effects in the pure d-superconductor [108]. In a number of microwave measurements the dependence $\Delta\lambda(T)$ becomes linear not in the immediate proximity of 4.2 K but at a higher temperatures (see, for example, curves $\lambda(T)$ in Fig. 9 for TBCCO and BKBO samples). But there are no systematic measurements on the dependence $\Delta\lambda(T)$ at $T < 5$ K.

§ The d-symmetry of the order parameter results from an interaction of alternating sign in the inverse space. Quasi-one-dimensional portions of the electron spectrum and the relevant van Hove singularities of HTSCs lead to d-pairing due to the anisotropic electron-phonon interaction [109]. Other origins of d-symmetry of the order parameter were considered in Refs [110, 11] within the phonon mechanism.

indicating the importance of the effect. For instance, the order parameter is shown in Ref. [132] to have mixed symmetry due to diffusion reflection from the surface: the original *d*-symmetry of the order parameter in the bulk of the superconductor is added to the *s*-component emerging near the surface. This may be a reason for the different dependences $\sigma_2(T)$ for YBCO crystals (Fig. 18) with approximately similar parameters characterizing the sample quality.

Thirdly, we have not considered a small piece of experimental data on the anisotropy of the surface impedance. To our knowledge, there is a single experiment [133], where the anisotropy of $Z_s(T)$ was observed in the *ab*-plane of YBCO single crystals without twins. There is some evidence that the dependences $Z_s(T)$ differ in the *ab*-plane and the *c*-direction [43, 45, 54, 55]. The theory [18, 103, 134 – 139] predicts different scenarios of high-frequency behaviour of HTSCs, caused by different mechanisms of anisotropy; therefore comparison with the precise microwave measurements would be useful.

The above questions are still not solved, and it seems likely that further experimental and theoretical studies of the microwave response in HTSCs are to be developed along these lines.

I am sincerely grateful to my colleagues and collaborators: experimenters (A A Zhukov, A T Sokolov, G É Tsydynzhapov), theorists (A A Golubov, O V Dolgov, S V Shul'ga), and materials technologists (L A Klinkova, N V Barkovskiĭ, G A Emel'chenko, I G Naumenko, N N Kolesnikov). V F Gantmakher has greatly promoted the studies, my discussions with him and E G Maksimov, D V Shovkun, and G M Eliashberg have been very useful. I remember the attentive concern and support of I F Shchegolev at the initial stage of these studies at ISSP. I am thankful to my collaborators from H Piel's laboratory (Wuppertal University), where I acquired experience in precise measurements of surface impedance in HTSCs. I am also thankful to S Sridhar and his colleagues from Northeastern University (Boston) for the facility offered of reproducing on their equipment the main features of the temperature dependences of the surface impedance of YBCO and TBCCO single crystals grown at ISSP.

These studies are carried out with the support of the RFBR (project 97-02-16836) and the Scientific Council on Superconductivity (project 96060).

References

1. Bardeen J, Cooper L N, Schrieffer J R *Phys. Rev.* **108** 1175 (1957)
2. Abrikosov A A, Gor'kov L P, Khalatnikov I M *Zh. Eksp. Teor. Fiz.* **35** 265 (1958) [*Sov. Phys. JETP* **8** 182 (1959)]
3. Mattis D C, Bardeen J *Phys. Rev.* **111** 412 (1958)
4. Turneaure J P, Halbritter J, Schwettman H A *J. Supercond.* **4** 341 (1991)
5. Klein O et al. *Phys. Rev. B* **50** 6307 (1994)
6. Trunin M R, Zhukov A A, Sokolov A T *Zh. Eksp. Teor. Fiz.* **111** 696 (1997) [*JETP* **84** 383 (1997)]
7. Eliashberg G M *Zh. Eksp. Teor. Fiz.* **38** 966 (1960) [*Sov. Phys. JETP* **11** 696 (1960)]
8. Marsiglio F *Phys. Rev. B* **44** 5373 (1991)
9. Olsson H K, Koch R H *Phys. Rev. Lett.* **68** 2406 (1992)
10. Golubov A A et al. *Physica C* **213** 139 (1993)
11. Horbach M L, van Saarloos W, Huse D A *Phys. Rev. Lett.* **67** 3464 (1991)
12. Anlage S M et al. *Phys. Rev. B* **53** 2792 (1996)
13. Dolgov O V et al. *Solid State Commun.* **89** 827 (1994)
14. Klimovich G V, Rylyakov A V, Eliashberg G M *Pis'ma Zh. Eksp. Teor. Fiz.* **53** 381 (1991) [*JETP Lett.* **53** 399 (1991)]
15. Gorter C J, Casimir H *Phys. Z.* **35** 963 (1934)
16. Mikhailovsky A A et al. *Solid State Commun.* **80** 511 (1991)
17. Orbach-Werbig S et al. *Physica C* **235 – 240** 2383 (1994)
18. Golubov A A et al. *Pis'ma Zh. Eksp. Teor. Fiz.* **62** 477 (1995) [*JETP Lett.* **62** 496 (1995)]
19. Liang R et al. *Physica C* **195** 51 (1992)
20. Hardy W N et al. *Phys. Rev. Lett.* **70** 3999 (1993)
21. Bonn D A et al. *Phys. Rev. Lett.* **68** 2390 (1992)
22. Sridhar S, Kennedy W L *Rev. Sci. Instrum.* **54** 531 (1988)
23. Altman J L *Microwave Circuits* (Princeton, N.J.: Van Nostrand, 1964) [Translated into Russian (Moscow: Mir, 1968)]
24. Kolesnikov N N et al. *Sverkhprovodimost': Fiz. Khim. Tekh.* **4** 957 (1991) [*SPCT* **4** (5) 867 (1991)]
25. Trunin M R et al. *Pis'ma Zh. Eksp. Teor. Fiz.* **65** 893 (1997) [*JETP Lett.* **65** 938 (1997)]
26. Poole C P *Electron Spin Resonance* (New York: Interscience Publ., a Division of John Wiley & Sons, 1967) [Translated into Russian (Moscow: Mir, 1970)]
27. Klinkova L A et al. *Sverkhprovodimost': Fiz. Khim. Tekh.* **7** 1437 (1994)
28. Trunin M R et al. *Pis'ma Zh. Eksp. Teor. Fiz.* **64** 783 (1996) [*JETP Lett.* **64** 832 (1996)]
29. Klein O et al. *Int. J. Infrared Millimeter Waves* **14** 2423 (1993)
30. Landau L D, Lifshitz E M *Elektrodinamika Sploshnykh Sred* (Electrodynamics of Continuous Media) (Moscow: Fizmatlit, 1982) [Translated into English (Oxford: Pergamon Press, 1960)]
31. Trofimov V N et al. *Physica C* **183** 135 (1991)
32. Gough G E, Exon N J *Phys. Rev. B* **50** 488 (1994)
33. Benkraouda M, Clem J R *Phys. Rev. B* **53** 5716 (1996)
34. Zeldov E et al. *Phys. Rev. Lett.* **73** 1428 (1994)
35. Indenbom M V, Brandt E H *Phys. Rev. Lett.* **73** 1731 (1994)
36. You H et al. *Phys. Rev. B* **38** 9213 (1988)
37. Meingast C et al. *Phys. Rev. B* **41** 11299 (1990)
38. Meingast C et al. *Phys. Rev. Lett.* **67** 1634 (1991)
39. Kierspel H et al. *Physica C* **262** 177 (1996)
40. Meingast C, Junod A, Walker E *Physica C* **272** 106 (1996)
41. Anshukova N V et al. *Fiz. Tverd. Tela* (Leningrad) **35** 1415 (1993)
42. Klein N et al. *Phys. Rev. Lett.* **71** 3355 (1993)
43. Mao J et al. *Phys. Rev. B* **51** 3316 (1995)
44. Jacobs T et al. *J. Phys. Chem. Solids* **56** 1945 (1995)
45. Kitano H et al. *Phys. Rev. B* **51** 1401 (1995)
46. Achkir D et al. *Phys. Rev. B* **48** 13184 (1993)
47. Zhang K et al. *Appl. Phys. Lett.* **62** 3019 (1993)
48. Bonn D A et al. *Phys. Rev. B* **50** 4051 (1994)
49. Annett J, Goldenfeld N, Renn S R *Phys. Rev. B* **43** 2778 (1991)
50. Ma Z et al. *Phys. Rev. Lett.* **71** 781 (1993)
51. Porch A, Lancaster M J, Humphreus R G *IEEE Trans. MTT* **43** 306 (1995)
52. de Vaulchier L A et al. *Europhys. Lett.* **33** 153 (1996)
53. Bonn D A, Hardy W N, in *Physical Properties of High-Temperature Superconductors V* Vol. 5 (Ed. D M Ginsberg) (Singapore: World Scientific, 1995) p. 7
54. Jacobs T et al. *Phys. Rev. Lett.* **75** 4516 (1995)
55. Shibauchi T et al. *Physica C* **264** 227 (1996)
56. Lee S F et al. *Phys. Rev. Lett.* **77** 735 (1996)
57. Zhukov A A et al. *Zh. Eksp. Teor. Fiz.* **112** 2210 (1997) [*JETP* **85** 1211 (1997)]
58. Broun D M et al. *Phys. Rev. B* **56** R11443 (1997)
59. Erb A, Walker E, Flukiger R *Physica C* **258** 9 (1996)
60. Srikanth H et al. *Phys. Rev. B* **55** R14733 (1997)
61. Srikanth H et al. *Phys. Rev. B* **57** 7986 (1998)
62. Hensen S et al. *Phys. Rev. B* **56** 6237 (1997)
63. Kamal S et al. *Phys. Rev. Lett.* **73** 1845 (1994)
64. Simonov V S, Molchanov V N *Kristallografiya* **41** 31 (1996)
65. Lobb C J *Phys. Rev. B* **36** 3930 (1987)
66. Fisher D S, Fisher M P A, Huse D A *Phys. Rev. B* **43** 130 (1991)
67. Salamon M B et al. *Phys. Rev. B* **47** 5520 (1993)
68. London F, London H *Proc. R. Soc. London Ser. A* **149** 71 (1935)
69. Nam S B *Phys. Rev.* **156** 470, 487 (1967)
70. Lifshitz E M, Pitaevskiĭ L P *Fizicheskaya Kinetika* (Physical Kinetics) (Moscow: Fizmatlit, 1979) [Translated into English (Oxford: Pergamon Press, 1981)]

71. Tinkham M *Introduction to Superconductivity* (New York: McGraw-Hill Book Co., 1975) [Translated into Russian (Moscow: Atomizdat, 1980)]
72. Abrikosov A A *Osnovy Teorii Metallov* (Fundamentals of the Theory of Metals) (Moscow: Fizmatlit, 1987) [Translated into English (Amsterdam: North-Holland, 1988)]
73. Waldram J R et al. *Phys. Rev. B* **55** 3222 (1997)
74. Ginzburg V L, Maksimov E G *Sverkhprovodimost'*: *Fiz. Khim. Tekh.* **5** 1543 (1992) [*SPCT* **5** (9) 1505 (1992)]
75. Eliashberg G M *Zh. Eksp. Teor. Fiz.* **39** 1437 (1960) [*Sov. Phys. JETP* **12** 1000 (1961)]
76. Karakozov A E, Maksimov E G, Mashkov S A *Zh. Eksp. Teor. Fiz.* **68** 1937 (1975) [*Sov. Phys. JETP* **41** 971 (1976)]
77. Karakozov A E, Maksimov E G, Mikhaĭlovskiĭ A A *Zh. Eksp. Teor. Fiz.* **102** 132 (1992) [*Sov. Phys. JETP* **75** 70 (1992)]
78. Collins R T, Schlesinger Z, Holtzberg F *Phys. Rev. B* **43** 3701 (1991)
79. Rammer J *Europhys. Lett.* **5** 77 (1988)
80. Shibauchi T et al. *Physica C* **203** 315 (1992)
81. Bonn D A et al. *Phys. Rev. B* **47** 11314 (1993)
82. Trunin M R, Zhukov A A, Sokolov A T *J. Phys. Chem. Solids* (to be published)
83. Dagotto E *Rev. Mod. Phys.* **66** 763 (1994)
84. Kampf A P *Phys. Rep.* **249** 219 (1994)
85. Scalapino D J *Phys. Rep.* **250** 329 (1995)
86. Shen Z X, Dessau D S *Phys. Rep.* **253** 1 (1995)
87. Loktev V M *Fiz. Nizk. Temp.* **22** 3 (1996)
88. Izyumov Yu A *Usp. Fiz. Nauk* **167** 465 (1997) [*Phys. Usp.* **40** 445 (1997)]
89. Ovchinnikov S G *Usp. Fiz. Nauk* **167** 1043 (1997) [*Phys. Usp.* **40** 993 (1997)]
90. Hirschfeld P J, Goldenfeld N *Phys. Rev. B* **48** 4219 (1993)
91. Hirschfeld P J, Putikka W O, Scalapino D J *Phys. Rev. Lett.* **71** 3705 (1993)
92. Hirschfeld P J, Putikka W O, Scalapino D J *Phys. Rev. B* **50** 4051 (1994)
93. Eliashberg G M, Klimovitch G V, Rylyakov A V *J. Supercond.* **4** 393 (1991)
94. Millis A, Monien H, Pines D *Phys. Rev. B* **42** 167 (1990)
95. Monien H, Monthoux P, Pines D *Phys. Rev. B* **43** 275 (1991)
96. Monthoux P, Balatsky A, Pines D *Phys. Rev. B* **46** 14803 (1992)
97. Lee P A *Phys. Rev. Lett.* **71** 1887 (1993)
98. Quinlan S M, Scalapino D J, Bulut N *Phys. Rev. B* **49** 1470 (1994)
99. Bille A, Scharnberg K *J. Phys. Chem. Solids* (to be published)
100. Kresin V Z, Wolf S A *Phys. Rev. B* **41** 4278 (1990); **46** 6458 (1992); **51** 1229 (1995)
101. Adrian S D et al. *Phys. Rev. B* **56** 7878 (1997)
102. Adrian S D et al. *Phys. Rev. B* **51** 6800 (1995)
103. Golubov A A et al. *J. Phys. I* (Paris) **6** 2275 (1996)
104. Klein N et al. *J. Supercond.* **7** 459 (1994)
105. Hein M, in *Studies of High-Temperature Superconductors* Vol. 18 (Ed. A Narlikar) (New York: Nova Sciences, 1996) p. 141
106. Srikanth H et al. *Physica C* **291** 235 (1997)
107. Schopohl N, Dolgov O V *Phys. Rev. Lett.* **80** 4761 (1998)
108. Kosztin I, Leggett A J *Phys. Rev. Lett.* **79** 135 (1997)
109. Abrikosov A A *Physica C* **214** 107 (1993); **222** 191 (1994); **244** 243 (1995)
110. Santi G et al. *Physica C* **259** 253 (1996)
111. Kamimura H et al. *Phys. Rev. Lett.* **77** 723 (1996)
112. Golubov A A (unpublished)
113. Combescot R, Leyronas X *Phys. Rev. Lett.* **75** 3732 (1995)
114. O' Donovan C, Carbotte J P *Phys. Rev. B* **52** 4568 (1995); **55** 8520 (1997)
115. Kim H, Nicol E J *Phys. Rev. B* **52** 13576 (1995)
116. Pokrovsky S V, Pokrovsky V L *Phys. Rev. B* **54** 13275 (1996)
117. Pashitskiĭ É A, Pentegov V I *Zh. Eksp. Teor. Fiz.* **111** 298 (1997) [*JETP* **84** 164 (1997)]
118. Wen X-G, Lee P A *Phys. Rev. Lett.* **80** 2193 (1998)
119. Gantmakher V F et al. *Pis'ma Zh. Eksp. Teor. Fiz.* **65** 834 (1997) [*JETP Lett.* **65** 870 (1997)]
120. Halbritter J *J. Supercond.* **5** 171 (1992); **5** 331 (1992); **8** 691 (1995)
121. Portis A M, in *Electrodynamics of High-Temperature Superconductors* (Lecture Notes in Physics Vol. 48) (Singapore: World Scientific, 1993)
122. Vendik O G, Popov A Yu *Philos. Mag. Lett.* **65** 219 (1992)
123. Mahel M *Solid State Commun.* **97** 209 (1996)
124. Velichko A V et al. *Physica C* **77** 101 (1997)
125. McDonald J, Clem J R *Phys. Rev. B* **56** 14723 (1997)
126. Jacobs T et al. *IEEE Trans. Appl. Supercond.* **7** 1917 (1997)
127. Matsumoto M, Shiba H *J. Phys. Soc. Jpn.* **64** 3384 (1995)
128. Tanaka Y, Kashiwaya S *Phys. Rev. Lett.* **74** 3451 (1996); *Phys. Rev. B* **53** 11957 (1996)
129. Bahkal S R *Phys. Rev. Lett.* **76** 3634 (1996)
130. Barash Yu S, Svidzinsky A A, Burkhardt H *Phys. Rev. B* **55** 15282 (1997)
131. Fogelström M, Rainer D, Sauls J A *Phys. Rev. Lett.* **79** 281 (1997)
132. Golubov A A, Kupriyanov M Yu *Pis'ma Zh. Eksp. Teor. Fiz.* **67** 478 (1998) [*JETP Lett.* **67** 501 (1998)]
133. Zhang K et al. *Phys. Rev. Lett.* **73** 2484 (1994)
134. Klemm R A, Liu S H *Phys. Rev. Lett.* **74** 2343 (1995)
135. Atkinson W A, Carbotte J P *Phys. Rev. B* **52** 10601 (1995); **55** 12748 (1997)
136. Abrikosov A A *Physica C* **258** 53 (1996)
137. Radtke R J, Kostur V N, Levin K *Phys. Rev. B* **53** R522 (1996)
138. Xiang T, Wheatley J M *Phys. Rev. Lett.* **76** 134 (1996); **77** 4632 (1996)
139. Hirschfeld P J, Quinlan S M, Scalapino D J *Phys. Rev. B* **55** 12742 (1997)